GEOMETRICALLY NONLINEAR FINITE ELEMENT ANALYSIS of a LATTICE DOME

by

Chiung-Yu Huang

Thesis submitted to the Faculty of the

Virginia Polytechnic Institute and State University

in partial fulfillment of the requirements for the degree of

Master of Science

in

Civil Engineering

APPROVED:

Dr. S. M. Holzer, Chairman

Dr. R. H. Plaut

Dr. J. R. Loferski

November 1989

Blacksburg, Virginia

GEOMETRICALLY NONLINEAR FINITE ELEMENT ANALYSIS of a LATTICE DOME

by

Chiung-Yu Huang

Dr. S. M. Holzer, Chairman

Civil Engineering

(ABSTRACT)

The geometry and the finite element method modelling of a lattice dome is presented.

Linear analyses and geometrically nonlinear analyses of the dome are performed. In addition, a buckling load prediction method is studied and extended to the multiple load distributions.

The results obtained from linear analyses are checked against the requirements of NDS, National Design Standard.

ACKNOWLEDGEMENTS

This work is dedicated to my family and my teachers. Among them, I am deeply indebted to Dr. S. M. Holzer for his teaching in both academy and personal life.

I appreciate Dr. R. H. Plaut and Dr. J. R. Loferski for participating on the committee and providing constructive suggestions.

The cooperation from computer consultant in VPI, has been crucial in the installation and the optimization of the analysis tool, ABAQUS.

The discussions with the graduate students in the department of Civil engineering at VPI, have been beneficial. Among them, Dr. J. F. Davalos and Con-Trong have contributed to this work. The association with the residents and staff in University Club has been enjoyable and educational.

Table of Contents

List of Illustrations

List of Tables

CHAPTER 1 Introduction

The principal goal of this study is to apply the commercial finite element software, ABAQUS, to investigate the behavior of a glued-laminated (glulam) lattice dome through all stages of loading up to collapse.

Because of its economical advantages and superior audio absorption ability, glulam timber domes have become a popular choice for assembly halls, stadiums, indoor swimming pools, etc. (Holzer, 1989). However, the structural analysis of the glulam dome has not evolved as much as its increasing popularity (Davalos, 1989). For example, the structural analysis of Varax domes (Varax) is confined to linear finite element analysis, and the structural analysis of Triax domes is performed with the matrix displacement method.

A study of current available analysis tools may provide an effective approach for performing nonlinear analysis of these domes. An effective analysis is expected to predict the complete structural response including the collapse load, and to deter-

mine whether the first limit state is caused by exceeding the material strength or the stability limit of the structure.

A clear understanding of the structural response of these domes may provide information about the safety and potential failure modes and lead to more effective utilization of glulam members.

ABAQUS was chosen as the analysis tool because of its B32 element, which is capable of modelling curved beams, and because of its excellent nonlinear analysis capabilities.

A buckling load prediction method (Chang, 1988) is studied and applied to provide the guideline for selecting the parameters which control the nonlinear analysis in ABAQUS. In addition, the method is extended to multiple load conditions.

This study presents the linear and geometrically nonlinear finite element analyses for a triax dome built in Raleigh, NC. The geometry of the triax dome is presented in chapter 2, the load conditions are defined in chapter 3, the modelling of the dome is considered in chapter 4, the nonlinear solution methods used in this study are discussed in chapter 5, and the element stresses are checked against the allowable values (NDS, 1986) in chapter 6. The results of the analyses are presented in chapter 7. Recommendations for future study and improvements in the accuracy of the analysis are presented in chapter 8.

CHAPTER 2 Geometry

2.1 Overview

According to the Triax report (Neal, 1973), the geometry of a Triax dome is completely defined by three triax parameters : the rise, the triax number, and the radius of its base ring. The geometry is first defined in a plane, called the pattern plane, then through a procedure this pattern is projected onto a spherical surface to obtain the 3-D geometry. The goal of this chapter is to present the details of the geometry of the dome and its symmetrical substructures.

In addition to the three triax parameters, the orientation of the cross section of a member in space has to be known in order to carry out structural analysis; in this study, the orientation is defined through a vector associated with the local $\vec{1}$ axis of the cross section. The derivation of this vector is presented in section 2.5.

The analysis of symmetrical substructures of the dome is discussed in section 2.6, and a local coordinate system associated with this application is presented. In addition, a simplified local coordinate system, which can avoid the complexity in boundary constraints of sub-structures, is presented in section 2.7.

2.2 Pattern plane

A pattern plane is a horizontal plane which provides the foundation of the triax projection. The plane consists of several rings of equilateral triangles, called the triax field.

As shown in Fig. 2.2, the triax field originates from a center which is the horizontal projection of the apex of the dome. From the center extend six equilateral triangles of the first ring. Then from the triangles of the first ring extend the triangles of the second ring and then the third ring and so on. The region of the pattern plane between the triax field and the tension ring is called the peripheral field. The peripheral field is triangulated to connect the triax field with the support ring.

The pattern plane can be decomposed into six sectors (Fig. 2.2), which reflect cyclic symmetry (section 2.6). The length of the equilateral triangles in the pattern plane is computed as follows :

$$l = \frac{r_{base}}{N} \qquad (2.2.1)$$

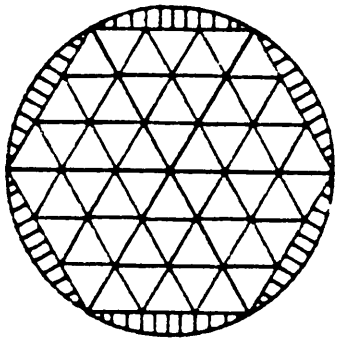

Triax Number = 3

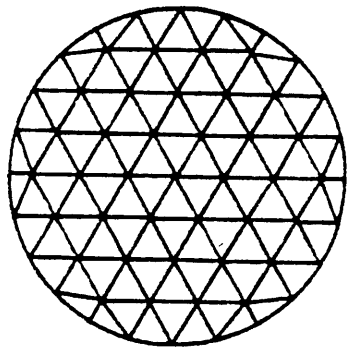

Triax Number = 3.5

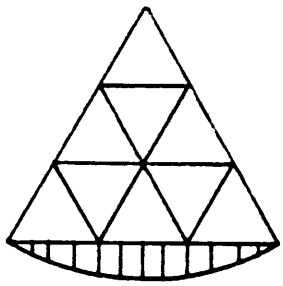

Pattern Sector

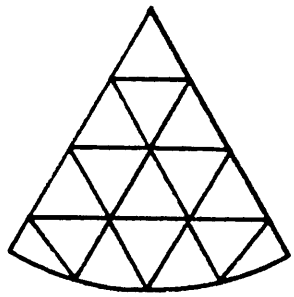

Pattern Sector

Figure 2.2 Pattern plane

where

l is the length of the triangle

r_{base} is the radius of the base ring

N is the triax number

Knowing the value of the triax number and the radius of the base ring, we can define the pattern plane. Once the pattern plane is defined, we can proceed to the next step, the projection.

2.3 Projection

To illustrate the procedure of projection, we draw a line from the center of the sphere, C, through a point, P, in the pattern plane. The intersection of this line and the sphere , point P', is the projection of that point, as shown in Fig. 2.3.

We need to know the radius of the sphere and the location of its center for the projection. This information can be extracted from the three triax parameters of a Triax dome, namely, the rise, h, the triax number, N, and the radius of the base, r_{base} .

Considering Fig. 2.3, we have the following geometrical relationships:

$$\tan \beta = \frac{r_{base}}{h} \qquad (2.3.1)$$

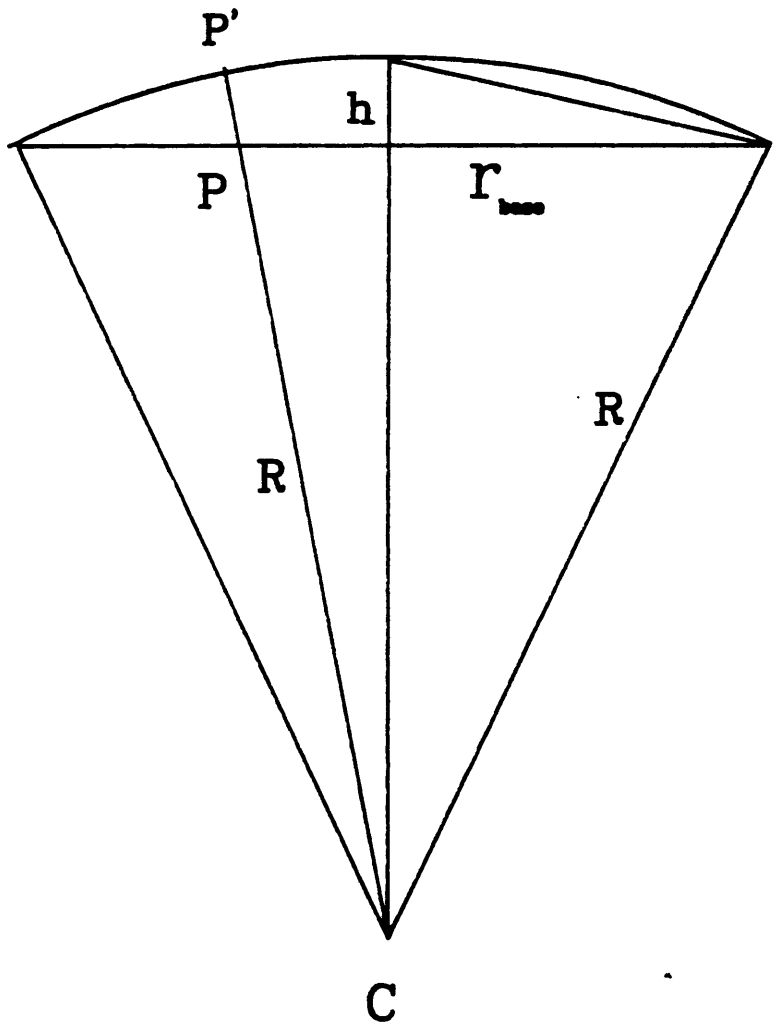

Figure 2.3 Projection

$$\alpha = 180^0 - 2\beta \tag{2.3.2}$$

$$h = R - R\cos\alpha \tag{2.3.3}$$

or

$$R = \frac{h}{1 - \cos\alpha} \tag{2.3.4}$$

Once the value of R is known the vector $\vec{CP'}$ can be computed as

$$\vec{CP'} = R\,\frac{\vec{CP}}{|\vec{CP}|} \tag{2.3.5}$$

Therefore, the location of the point P' is determined.

2.4 Tension ring

The perimeter of the dome is confined by a ring, which is stressed in tension (Neal, 1973). The tension ring is usually made of steel plates, although concrete or wood materials are used occasionally. It is suggested that the tension ring should be composed of straight members to eliminate eccentric ring moments. The tension ring is modelled with truss elements in this study.

2.5 Local 1 axis

The orientation of a member in space is defined through a vector called local 1 axis of the cross section. The local 1 axis of a rectangular cross section is a vector along the width of the element as shown in Fig. 2.5.

In a Triax dome, all the structural members lie in great circles. A great circle is formed by the intersection of a plane passing through the center of a sphere. Because of this characteristic, the local 1 axis of any member of the dome can be expressed by the following equation:

$$\vec{1} = \frac{\vec{CA} \times \vec{CB}}{|\vec{CA} \times \vec{CB}|} \qquad (2.5.1)$$

where A and B are the end points of a member of the dome.

2.6 Symmetrical substructures and local coordinate system

The analysis of a symmetrical structure can be simplified by confining it to a sub-structure isolated along elements of symmetry (Holzer, 1985). The computational effort measured by the CPU time, and the required size of memory can be reduced significantly by the employment of symmetry in structures. The dome is divided into six symmetrical substructures, called sectors as shown in Fig. 2.6. The boundaries

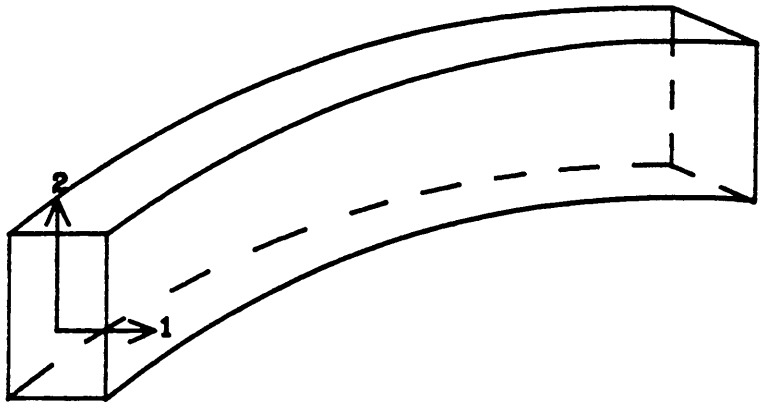

a. Local 1 axis of the cross section of a beam section

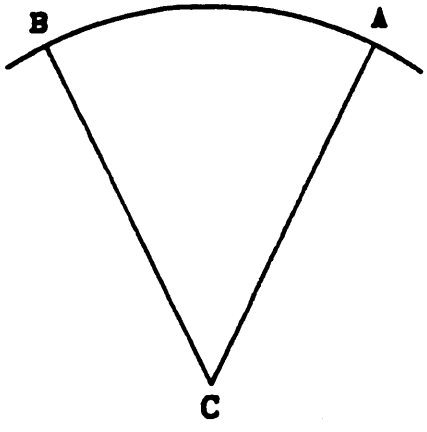

b. Element in a great circle

Figure 2.5 Local 1 axis

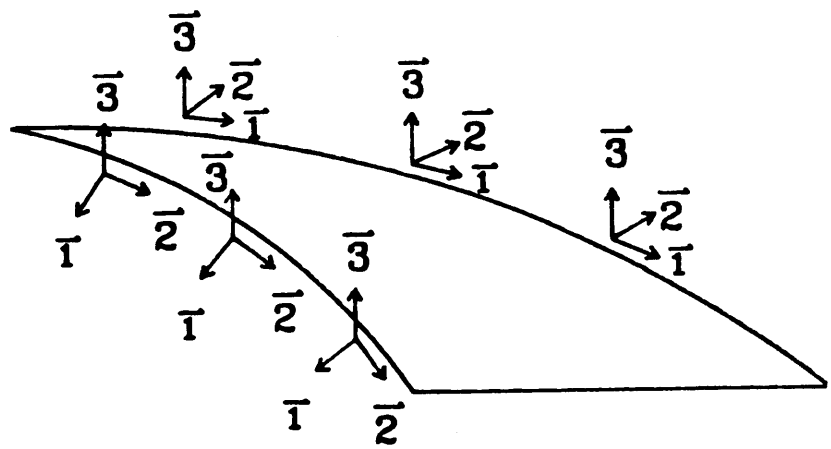

Figure 2.6 A symmetrical sub-structure and a local coordinate system

between adjacent sectors are called divisor lines (Neal, 1973). The axes of nodal coordinate system $\vec{1}$, $\vec{2}$, and $\vec{3}$ are defined as follows: the $\vec{2}$ and $\vec{3}$ axes lie in the great circle plane -- the $\vec{2}$ axis is tangential and the $\vec{3}$ axis is normal to the divisor line -- and the $\vec{1}$ axis is perpendicular to the great circle plane.

In addition to cutting the widths of the members on the divisor lines in half, boundary constraints have to be applied to the nodes on the divisor lines in order to simulate the effect of the surrounding structure. Fig. 2.6 indicates that symmetry requires the following constraints : no deflection in the $\vec{1}$ direction and no rotations about the $\vec{2}$ and $\vec{3}$ axes.

2.7 Simplified local coordinate systems

The local coordinate system presented in the previous section is not efficient because each node on the divisor line requires its own local coordinate system. Moreover, the nodes at intersections between the divisor lines and the base ring need to be constrained in the vertical direction. This constraint requires either introducing another coordinate system at these nodes with an axis in the vertical direction, or, using a very stiff truss element to simulate the roller mechanism at these nodes.

This set of boundary constraints is rather complicated and a simplification is suggested by Holzer and Davalos. The local $\vec{1}$ axis of the simplified local coordinate system is normal to the great circle plane containing the divisor line. The local $\vec{3}$ axis is vertical and the local $\vec{2}$ axis is selected to make the axes mutually orthogonal (i.

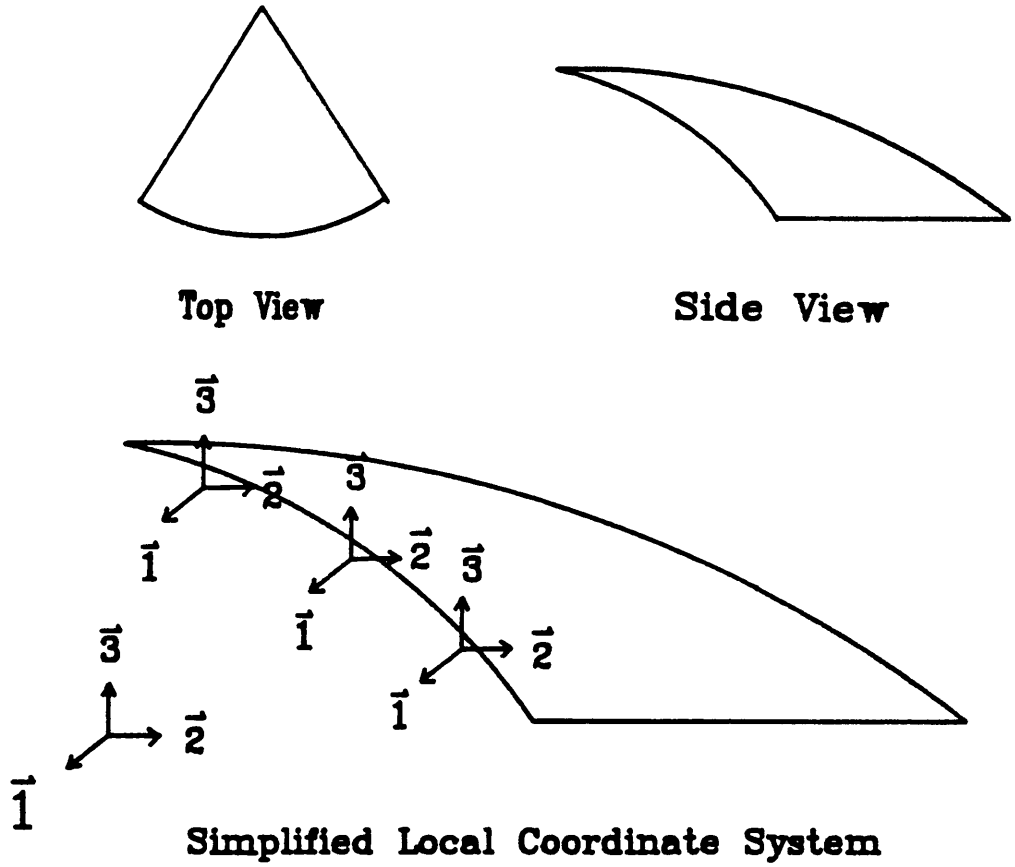

Figure 2.7 Simplified local coordinate system

e., it is horizontal). Symmetry again requires the following constraints: no deflection in the direction of the $\vec{1}$ axis and no rotations about the $\vec{2}$ and $\vec{3}$ axes.

CHAPTER 3 Load

3.1 Overview

The goal of this chapter is to obtain the nodal force vector of the dome for different design load combinations. The nonlinear solution algorithms and the strategy to find the critical load are discussed in chapter 5.

Several different types of loads and the corresponding design values are discussed in section 3.2. The various combinations of loads are discussed in section 3.3. The discretization of distributed loads into concentrated nodal forces is presented in section 3.4.

3.2 Different types of loads

The loads that need to be taken into account in structural analysis include dead load, live load, snow load, impact load and seismic load (AITC, 1985). Among all the above mentioned loads, heavy local snow concentrations appear to be most important; they have caused several failures of lattice domes (Holzer, 1989).

3.2.1 Dead load

Dead load is the weight of structural members and permanent facilities (AITC, 1985). Generally, dead load includes the contributions from the structural members, such as beams and purlins, the steel connectors, the tongue-and-groove decking, insulation and roofing material, and mechanical and electrical facilities (Neal, 1973).

The American Institute of Timber Construction, AITC, provides two tables for estimating the weights of construction materials (Table 3.1 and Table 3.2). The dead load is estimated to be 16 psf, which includes 2 psf of beams and purlins, 5 psf of decking (2 inches in thickness), and 9 psf steel for connectors, roofing, and insulation materials (Davalos, 1989).

3.2.2 Live load

The live load is the weight imposed by the use or occupancy of the structure except wind, snow, and seismic loads. A table of minimum uniformly distributed roof live loads is given in Table 3.5 AITC. The value of minimum roof live load depends upon the slope of the roof and its tributary loaded area. The live load is estimated as 20 psf (Davalos, 1989).

The weight of hanging lighting facilities and any other locally concentrated devices is not considered in this study.

3.2.3 Snow load

Factors affecting snow load accumulation on the roofs include the variations of elevation, latitude, wind frequency, duration of snowfall, roof geometry, and site exposure. The values of ground snow load are available in Fig. 3.1 of the AITC manual, and the roof snow load can be obtained from that figure with adjustment for roof geometry and wind exposure.

The snow load is estimated to be 20 psf (Davalos, 1989).

3.2.4 Wind load

According to AITC, the value of the wind load acting on a structure depends primarily upon the wind velocity. AITC provides a map of velocity for structures in different geographic locations. The value of the wind velocity has to be adjusted for the heights of structures. Once the adjusted wind velocity is known, the velocity pressure is computed. Finally the design wind pressure distribution is obtained by multiplying the velocity pressure with a pressure coefficient. AITC also provides a table of pressure coefficients.

A wind velocity map for air flow in open, level country at a height of 30 ft above the ground is given in section 3 of the AITC manual. The wind velocity is then required to be adjusted by the height formula

$$V_h = V_{30} \left[\frac{h}{30} \right]^{\frac{1}{x}} \qquad (3.2.1)$$

where

V_h is the wind velocity at any height

V_{30} is the wind velocity at a height of 30 ft

h is the height

x is a value that varies from 3 to 7, depending upon general site exposure conditions

The velocity pressure is then computed as

$$q = 0.00256\ V_h^2 \qquad (3.3.2)$$

where

q is the velocity pressure in terms of psf

V is the wind velocity in terms of miles per hour

The design wind pressure distribution acting on a structural element is obtained by multiplying the velocity pressure with a pressure coefficient, C_p. The value of C_p is provided by AITC in a tabulated format (Table 3.8, AITC).

3.2.5 Seismic load

The discussion on seismic load is available in section 3 of the AITC manual.

3.3 Load combinations

In section 3.2, we discussed the various types of loads under consideration; however, in order to obtain design loads for structural analyses, various combinations of different types of loads have to be studied as required by AITC.

The following seven combinations are suggested in the Varax report (Varax)

1. Combined dead load and live load over the entire dome
2. Combined dead load and live load on half of the dome terminating on sector lines

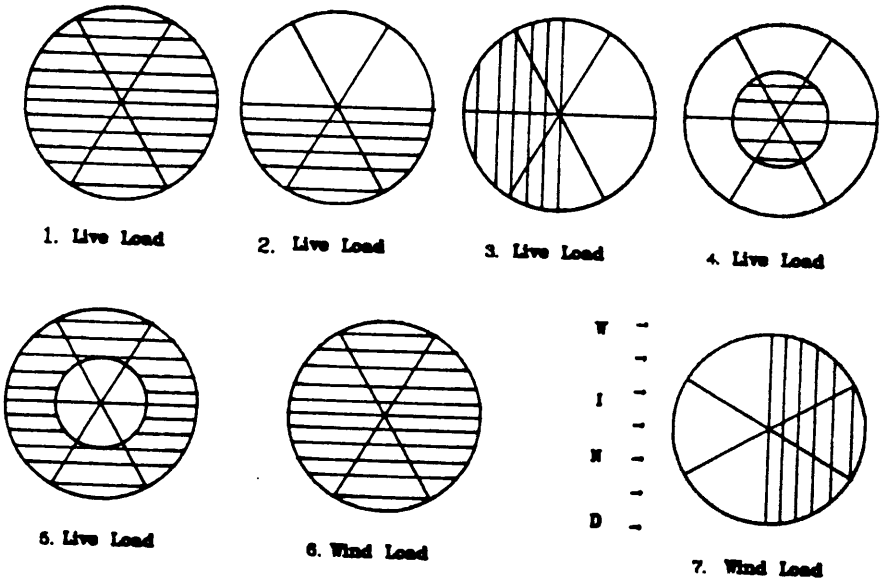

Figure 3.3 Load combination

3. Combined dead load and live load on half of the dome terminating on sector center lines
4. Combined dead load and live load on the inner half of the dome
5. Combined dead load and live load on outer half of the dome
6. Combined dead load and wind load
7. Combined dead load, wind load, and the live load on half of the dome on the leeward side

The shaded areas of Figure 3.3 show the regions of the applied live and wind loads of these load cases.

3.4 Discretization of loads

Except concentrated loads, all the applied loads, such as dead load, live load, snow load, and seismic loads, are distributed loads and defined per unit horizontal projection area. In order to carry out finite element analyses, these distributed loads have to be discretized into sets of nodal forces.

A typical panel of the mesh and the tributary area of each member in the panel are shown in Fig. 3.4. The tributary area is chosen on the basis that the load applied to a strip of the decking is assumed to be equally transferred to the end supports of the strip. Then the distributed loads along the members of the panel are discretized into nodal forces. Finally the nodal forces of each panel are assembled into a nodal force

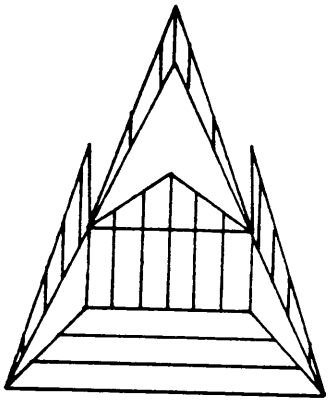

a. Tributary Area

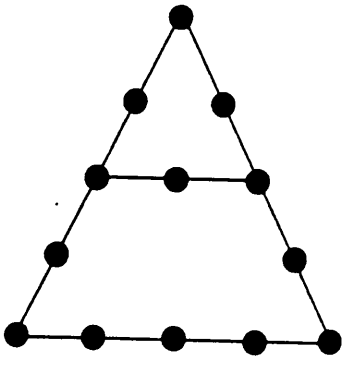

● Nodal forces

b. Discretized panel loads

Figure 3.4 Discretization of loads

vector of the dome. The discretization utilizes the Lagrange interpolation functions for a 3-noded element (Holzer, 1985) :

$$
\begin{aligned}
l_1(\xi) &= \frac{\xi(\xi - 1)}{2} \\
l_2(\xi) &= -(1 + \xi)(\xi - 1) \\
l_3(\xi) &= \frac{\xi(\xi + 1)}{2}
\end{aligned}
\qquad (3.5.1)
$$

Two Fortran programs have been written: one discretizes the applied loads for each panel (Appendix A), and the other assembles the nodal forces into a system nodal force vector panel by panel (Appendix B).

CHAPTER 4 Model

4.1 Overview

In this chapter, modelling for the linear analyses of the dome and the solution technique are discussed. The choice of elements in the mesh is discussed in section 4.2. The assumptions of the B32 element and the ABAQUS input data format of a B32 element are presented in section 4.3. The assumptions of the C1D2 element and the input data format of a C1D2 element are presented in section 4.4. The removal of rigid body motions of the model is discussed in section 4.5. The Frontal Solver, which is used in ABAQUS to solve the simultaneous algebraic equations, is briefly discussed in section 4.6.

4.2 The choice of elements in the mesh

ABAQUS provides six types of beam elements for 2-D analyses and seven types of beam elements for 3-D analyses. Since the analyses in this study are considered to be 3-D, the beam elements used in the mesh should be chosen from the 3-D beam elements. Among the seven types of 3-D beam elements, three are based on hybrid formulation, which is intended for the analysis with very slender or very stiff beams (ABAQUS, 1988). Therefore the hybrid 3-D beam elements are not suitable for this study.

A 3-D isobeam element, B32 in ABAQUS, is chosen to model the curved wood members of the dome because of its quadratic interpolation associated with three nodes and its ability to include shear deformations. The quadratic interpolation is necessary to model the curves of beams and purlins. Because shear deformation is significant in wood material, shear effects must be included in the element's formulation.

As mentioned in section 2.4, the main function of the steel tension ring is to absorb the induced tensile force along the base ring of the dome. Without a steel tension ring, the dimensions of the wood member in the base ring would have to be increased significantly to carry the developed axial forces in the base ring. Since the primary function of the steel tension ring is to carry axial force, the tension ring can be modelled with truss elements, C1D2 in ABAQUS.

Although the radial stress is responsible for several failures of pitched-tapered glulam beams, the effect of radial stress can be neglected when the curvature is considered to be large (Davalos, 1985). In this study, the radius of curvature of

members is 220 ft. The curvature is considered to be large; therefore, the radial stress plays no role in the selection of elements.

4.3 B32 Beam element

The assumptions involved in the formulation of the B32 beam elements are:

1. The cross section of the element remains plane before and after deformation but not necessarily normal to the reference axis.
2. No deformation in the plane of cross section; i.e., the warpping effect is not incorporated in the B32 element.
3. Quadratic interpolation functions are used for discretization.
4. The response in transverse shear is assumed to be linearlly elastic at all time; i.e., material nonlinearity is not included in the formulation.

The ABAQUS input data for the B32 beam element in Fig. 4.3, with lb-in as its units, are

```
*NODE
1, 0., 0., 0.
2, 1., 0., 0.
3, 2., 0., 0.
*ELEMENT, TYPE=B32, ELSET=EL1
1, 1, 2, 3
*BEAM SECTION, SECTION=RECT, MATERIAL=WOOD, ELSET=EL1
```

0.5000E+01, 0.1100E+02

0., 0., -1.

*MATERIAL, NAME=WOOD

*ELASTIC

1.8E+06, 4.625

*DENSITY

5.7E-05

As an ABAQUS's convention, the * sign always precedes key words such as NODE, ELEMENT, etc.. The NODE key word introduces the node number and the coordinates of a node. The ELEMENT key word introduces the type of element, the element number, and the node numbers. The BEAM SECTION key word introduces the section type, material, dimensions of the cross section, and the direction cosine of the local $\vec{1}$ axis (section 2.5) of the element. The MATERIAL key word introduces Young's modulus and Poisson's ratio of the material. In fact, the constitutive law of this element is defined through this keyword. The DENSITY key word introduces the density of the material.

It is worthy to mention the value of the Poisson's ratio, v, used here. The shear modulus, G, of an elastic, homogeneous, and isotropic material is usually expressed in terms of its Poisson's ratio and Young's modulus, E, as

$$G = \frac{E}{2\,(1+v)} \tag{4.3.1}$$

In ABAQUS, the user specifies the Poisson's ratio, and the program then computes the shear modulus. For the E-rated 56 southern pines, the Young's modulus is

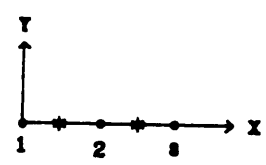

• Node

* Gauss Point

a. Node numbering

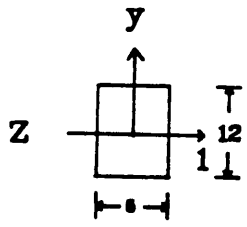

b. Dimension

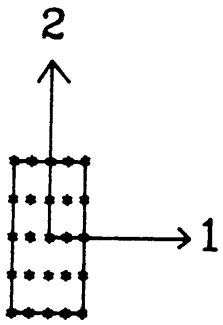

C. Newton–Cotes points

Figure 4.3 B32 element

1,800,000 psi and the shear modulus is 160,000 psi. The Poisson's ratio, which is required by ABAQUS, is computed by the equation (4.3.2), and yields the value 4.625. (Even though equation (4.3.2) does not apply to wood.)

$$v = \frac{E}{2G} - 1 \qquad (4.3.2)$$

Although the B32 element uses 25 Newton-Cotes points for numerical integration across its cross section (as shown in Fig. 4.3) it gives element stresses only at the four corners unless the user requests stresses at other points.

4.4 C1D2 truss element

The assumptions involved in the formulation of C1D2 elements are:

1. Deformations take place in the axial direction only.
2. The isoparametric interpolation function of the element is

$$u(\xi) = \frac{1}{2}(1-\xi)\,u_1 + \frac{1}{2}(1+\xi)\,u_2 \qquad (4.4.1)$$

3. The element is incompressible, i.e.,

$$a\,dl = A\,dL \qquad (4.4.2)$$

where a and l are the area and the length of the element in the current configuration, and A and L are the area and the length of the element in the reference configuration.

The ABAQUS input data for a C1D2 element in Fig 4.4 with lb-in as its units are

```
*NODE
1, 0., 0., 0.
2, 1., 0., 0.
*ELEMENT, TYPE=C1D2, ELSET=TRUSS
1, 1, 2
*SOLID SECTION, MATERIAL=STEEL, ELSET=TRUSS
12.
*MATERIAL, NAME=STEEL
*ELASTIC
2.9E+07, 0.3
*DENSITY
7.3E-04
```

The area of the truss element is defined through the keyword SOLID SECTION to be 12. The stress of a C1D2 element is given at the Gauss point of the element.

4.5 Removal of rigid body motion

The rigid body modes of all the ABAQUS elements are imbedded in the formulations of the elements; the user has no control over them. The discussion of these rigid body modes can be found in the ABAQUS theory manual (ABAQUS, 1988). On the other hand, the user is responsible to restrain the dome from rigid body motion. Se-

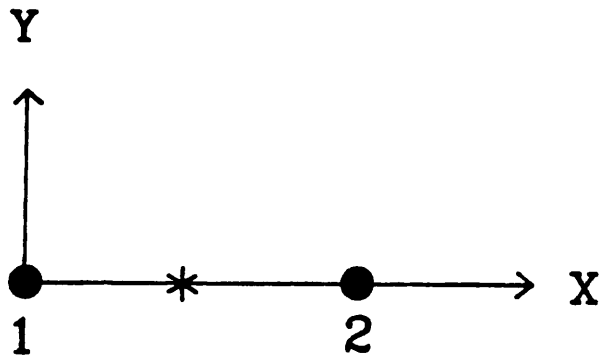

● Node

* Gauss Point

a. Node ordering

Note : C1D2 element is cross -section shape independent

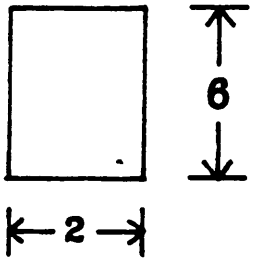

b. Area

Figure 4.4 C1D2 element

veral types of boundary constraints are possible to eliminate the dome's rigid body motions. In this study, two different types of boundary constraints are examined and the results are discussed.

In the type 1 constraints, shown in Fig. 4.5, the constraints in the 3 direction applied to the nodes in the base ring remove the rigid body motion in the 3 direction. The constraint applied to nodes 38 and 50 in the 1 direction remove the rigid body motion in the 1 direction. The constraints in the 2 directions applied to the nodes 44 and 56 remove the rigid body motion in the 2 direction. The rotation about the 3 direction is automatically removed because of the constraints in the 1 and 2 directions. As the result, the nodes in the base ring are free to expand radially in the horizontal plane containing the base ring, and all the other nodes are free to deform in any degree of freedom.

In the type 2 constraints, shown in Fig. 4.5, the constraints in the 3 direction applied to the nodes in the base ring remove the rigid body motion in the 3 direction. The constraints in 1 and 2 directions applied to the node 1 remove the the rigid body motion in 1 and 2 directions respectively. The rotation about the 3 direction is removed by the constraint at node 1 in that direction. As the result, the nodes in the base ring are free to expand in the horizontal plane containing the base ring, the apex is allowed to deform only in the 3 direction and rotations about the 1 and 2 directions, although symmetry itself should force the rotation not to take place.

Type 1 and type 2 constraints are expected to yield the same results in nodal displacements and element stresses, but differences are observed. The dome with type 2 constraints fails to respond symmetrically under symmetrical loads but the dome with type 1 constraints does provide symmetrical response under symmetrical loads.

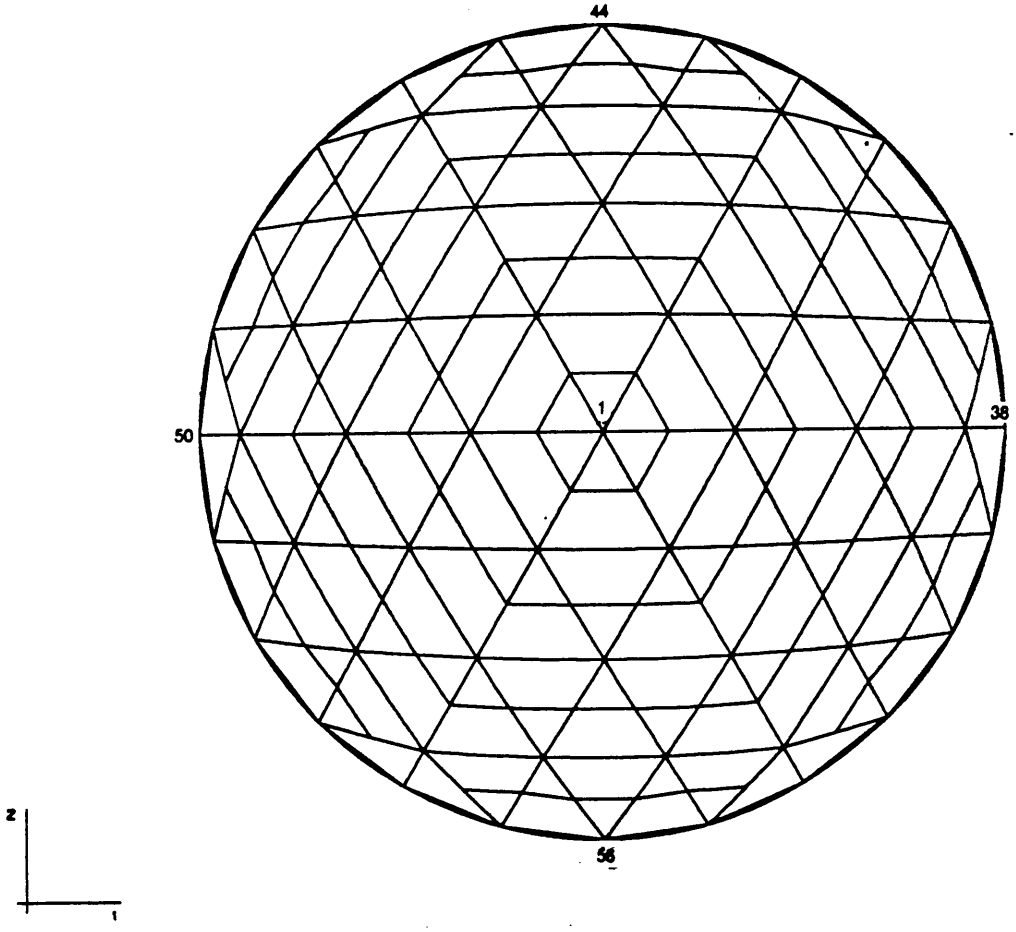

Figure 4.5 Boundary constraints

Therefore, type 1 boundary constraints are chosen for the rest of study. The incorrect response of the dome with type 2 constraints is attributed to the accumulation of computational errors.

4.6 Frontal solver

Once the mesh is established, the element stiffness matrices can be assembled into the system stiffness matrix, and the dome is represented by the system of simultaneous equations

$$K\,q \;=\; Q \qquad (4.6.1)$$

where

K is the system stiffness matrix

q is the nodal displacement vector

Q is the nodal load vector

Several methods have been proposed to solve the above equation in different ways to meet the constraints of the available computing facilities, such as the size of central memory and the size of out-of-core memory.

The most popular methods in engineering practice are direct methods which use out-of-core memory as the secondary storage. Among the variations of direct methods, out-of-core band solver and frontal solver are the most widely used.

The out-of-core band solver, an application of Gaussian elimination, requires the system stiffness matrix to be completely assembled before equations are solved. The frontal solver, another application of Gaussian elimination, can solve the simultaneous equations even before they are completely assembled.

The frontal solver utilizes two features from standard Gaussian elimination : 1. The coefficients of the *k th* equation are fully summed after the last finite element that contains the *k th* variable has been assembled. 2. When the coefficients of the *k th* equation are fully summed, the *k th* variable can be eliminated.

In fact, the frontal solver proceeds element by element, analogous to a wave passing over a structure. A variable becomes active on its first appearance; it is then moved into central memory, and is immediately eliminated on its last appearance ; the room occupied by this coefficient can then be released to other coefficients.

The efficiency of the frontal solver depends on the ordering of elements, whereas the efficiency of the out-of-core band solver depends on the ordering of nodes.

Demonstrative examples of how the frontal solver alternates between assembling elements and eliminating degrees of freedom are available in Bathe (1983) and Holzer (1985).

CHAPTER 5 Geometrically Nonlinear Analysis

5.1 Overview and proportional loading

The study of the nonlinear behavior of a structure is recommended when the relation between the displacements and the applied load is not linear (Bathe, 1982). Although the nonlinear behavior of a structure may come from many sources such as material properties (known as material nonlinearity), the condition of boundary contact (known as contact problems), the change in the geometry (known as geometrical nonlinearity), we only consider geometrical nonlinearity in this study.

Proportional loading is used throughout the nonlinear analyses in this study. The applied load, Q, is obtained by multiplying a scalar λ, with a load vector, $\overline{Q}$, which remains unchanged in the analysis, as in the following equation :

$$Q = \lambda \overline{Q} \tag{5.1.1}$$

where λ is called load parameter or load proportionality factor.

The nonlinear solution schemes used in this study are the modified Newton-Raphson method and the Riks-Wempner method; they are discussed in sections 5.2 and 5.3 respectively. A discussion of buckling load prediction is presented in section 5.4. Buckling load predictions in both single and multiple load distributions are discussed in section 5.5. Finally a strategy for conducting a nonlinear analysis with ABAQUS is discussed in section 5.6, and a flow chart is presented.

5.2 Modified Newton-Raphson Method

The presentation in this section is based on Bathe (1983).

The equilibrium of a structure requires that the following equation be maintained through the analysis :

$$^{t}Q - {}^{t}F = 0 \tag{5.2.1}$$

where t denotes time in dynamic analysis; it is an artificial variable in static analysis. Q is the external nodal force vector, and F is the internal nodal force vector, which is equivalent to the element stresses corresponding to the configuration ^{t}q.

When proportional load is used, the applied load is magnified through a load parameter. However due to the nonlinearity, the nodal displacements do not grow at the same rate as the applied load. Consequently neither does the nodal force vector, ^{t}F. Therefore an increase in the applied load creates a difference between ^{t}Q, and ^{t}F; the difference is called the out-of-balance force vector or the unbalanced force

vector. Equilibrium requires the out-of-balance force vector to be zero as shown in equation (5.2.1). But in practice, once the difference is smaller than a specified error tolerance, we consider equilibrium is achieved. We use several iterations to reduce the difference between ${}^{t}Q$ and ${}^{t}F$. The rest of this section discusses one of the iteration methods used in this study, the Newton-Raphson method.

To begin with, we assume the nodal displacement vector, ${}^{t+\Delta t}q^{(0)}$, and the nodal force vector, ${}^{t+\Delta t}F^{(0)}$, to be known at the beginning of a time increment Δt:

$$ {}^{t+\Delta t}q^{(0)} = {}^{t}q \tag{5.2.2} $$

$$ {}^{t+\Delta t}F^{(0)} = {}^{t}F \tag{5.2.3} $$

where ${}^{t}q$, and ${}^{t}F$ are the nodal displacement and nodal force vectors at the end of the previous increment.

Increasing the load from ${}^{t}Q$ to ${}^{t+\Delta t}Q$, we obtain the unbalanced force vector in the $i-th$ iteration as

$$ R^{(i-1)} = {}^{t+\Delta t}Q - {}^{t+\Delta t}F^{(i-1)} \tag{5.2.4} $$

For the reason of computational efficiency, the modified Newton-Raphson method does not update the tangent stiffness matrix at each iteration. Instead, the tangent stiffness matrix of the initial configuration of the increment, ${}^{t}K$, is used through all the iterations in the same increment. Now we solve for Δq^{i}, which is the increase in the nodal displacement vector due to the unbalanced force vector, by the following equation :

$$ {}^{t}K \quad \Delta q^{i} = R^{(i-1)} \tag{5.2.5} $$

Next we update the nodal displacement vector by the following equation :

$$^{t+\Delta t}q^{i} = {}^{t+\Delta t}q^{(i-1)} + \Delta q^{i} \qquad (5.2.6)$$

We compute the nodal force vector, $^{t+\Delta t}F^{(i)}$, corresponding to the current configuration $^{t+\Delta t}q^{(i)}$. Then, we compute $R^{(i)}$ by the equation (5.2.4), and stop further iterations if $R^{(i)}$ is smaller than the specified error tolerance; otherwise we proceed to the next iteration.

The load increment can be adjusted by the program itself based upon the rate of convergence as in ABAQUS. The tangent stiffness matrix, ^{t}K , can be replaced by the updated stiffness matrix from iteration to iteration as the Newton-Raphson method does. However, the extra effort in computing and factorizing the updated stiffness does not always offset the improvement in the rate of convergence.

5.3 Riks-Wempner Method

The presentation in this section is based on Holzer (1982).

In the Riks-Wempner method, a state is designated in the load-displacement space by the vector

$$r = \begin{bmatrix} \lambda \\ q \end{bmatrix} \qquad (5.3.1)$$

where λ is the load parameter and q is the nodal displacement vector.

Incorporating a variable load parameter, the Riks-Wempner method utilizes the following incremental equilibrium equation :

$$K^{(i-1)} \Delta q^{(i)} = \Delta \lambda^{(i)} \overline{Q} + R^{(i-1)} \tag{5.3.2}$$

where

i is the iteration counter

$K^{(i-1)}$ is the tangent stiffness matrix

$\Delta q^{(i)}$ is the incremental nodal displacement vector

$\Delta \lambda^{(i)}$ is the incremental load parameter

$R^{(i-1)}$ is the residual (unbalanced) nodal force vector

$\overline{Q}$ is the constant load vector

If the load parameter remains constant during iteration, *i.e.*, $\Delta \lambda^{(i)} = 0$, equation (5.3.2) reduces to

$$K^{(i-1)} \Delta q^{(i)} = R^{(i-1)} \tag{5.3.3}$$

which corresponds to the Newton-Raphson method.

The first trial solution is defined by the vector

$$\Delta r^{(0)} = \begin{bmatrix} \Delta \lambda^{(0)} \\ \Delta q^{(0)} \end{bmatrix} \tag{5.3.4}$$

where

$$\Delta \lambda^{(0)} = \pm \Delta S \, / \, (\Delta q^{(0)^T} \cdot \Delta q^{(0)} + 1)^{\frac{1}{2}} \tag{5.3.5}$$

and

$$\Delta q^{(0)} = \Delta \lambda^{(0)} \Delta q^{(0I)} \tag{5.3.6}$$

where ΔS is the arc length and $\Delta q^{(0I)}$ is the solution of

$$K^{(0)} \Delta q^{(0I)} = \bar{Q} \tag{5.3.7}$$

Subsequent iterations take place on a " normal plane " and are based on the following equations:

$$q^{(i)} = q^{(i-1)} + \Delta q^{(i)} \tag{5.3.8}$$

$$\lambda^{(i)} = \lambda^{(i-1)} + \Delta \lambda^{(i)} \tag{5.3.9}$$

$$\Delta q^{(i)} = \Delta \lambda^{(i)} \Delta q^{(iI)} + \Delta q^{(iII)} \tag{5.3.10}$$

$$K^{(i-1)} \Delta q^{(iI)} = \bar{Q} \tag{5.3.11}$$

$$K^{(i-1)} \Delta q^{(iII)} = R^{(i-1)} \tag{5.3.12}$$

$$\Delta \lambda^{(i)} = -\frac{\Delta q^{(0)^T} \cdot \Delta q^{(iII)}}{\Delta q^{(0)^T} \cdot \Delta q^{(iI)} + \Delta \lambda^{(0)}} \tag{5.3.13}$$

5.4 Buckling load prediction

The two essential operations of buckling load prediction suggested by Chang (1988) are eigenvalue computation and extrapolation based upon the obtained eigenvalues.

The eigenvalue problem comes from the change of the system stiffness matrix due to the change in the applied loads. The detailed procedure is as follows :

1. Apply a base load, ${}^{B}Q$, and obtain the corresponding tangent stiffness matrix ${}^{B}K$ through a nonlinear analysis.
2. Apply a small load increment, ΔQ, to define the reference load

$$ {}^{R}Q = {}^{B}Q + \Delta Q \tag{5.4.1} $$

The corresponding tangent stiffness matrix is denoted as ${}^{R}K$.

3. According to the linear buckling theory, it is assumed that for any load

$$ Q = {}^{B}Q + \lambda \Delta Q \tag{5.4.2} $$

the corresponding stiffness matrix is

$$ K = {}^{B}K + \lambda \Delta K \tag{5.4.3} $$

where the incremental stiffness matrix $\Delta K = {}^{R}K - {}^{B}K$ is used in ABAQUS.

4. Solving λ from the eigenvalue problem

$$ ({}^{B}K + \lambda \Delta K) \Phi = 0 \tag{5.4.4} $$

we obtain λ_{CR}, the critical load parameter. Consequently we have the buckling mode ϕ_{CR} and the buckling load

$$Q_{CR} = {}^{B}Q + \lambda_{CR} \Delta Q \tag{5.4.5}$$

5.5 Buckling prediction in single and multiple load distributions

In the nonlinear analysis, the load increment may or may not share the same distribution as the base load distribution. A structure is subject to single load distribution if its load increment and base load have the same distributions; it is subject to multiple load distributions if the load distributions are different.

For single load distribution, the applied load, Q, can be expressed as follows :

$$Q = \lambda_B \, {}^{B}Q \qquad 1 \leq \lambda_B \leq \lambda_{CR} \tag{5.5.1}$$

where the base load ${}^{B}Q$ is magnified by λ_B from 1 to λ_{CR}.

As λ_B approaches λ_{CR}, we obtain a sequence of critical load parameter predictions converging to λ_{CR}. If we draw a 45 degree line from the origin of the coordinate system as shown in Fig. 5.5.1, the intersection between this line and the curve through all the critical load predictions is the predicted λ_{CR}. The predicted buckling load is

$$Q_{CR} = \lambda_{CR} \, {}^{B}Q \tag{5.5.2}$$

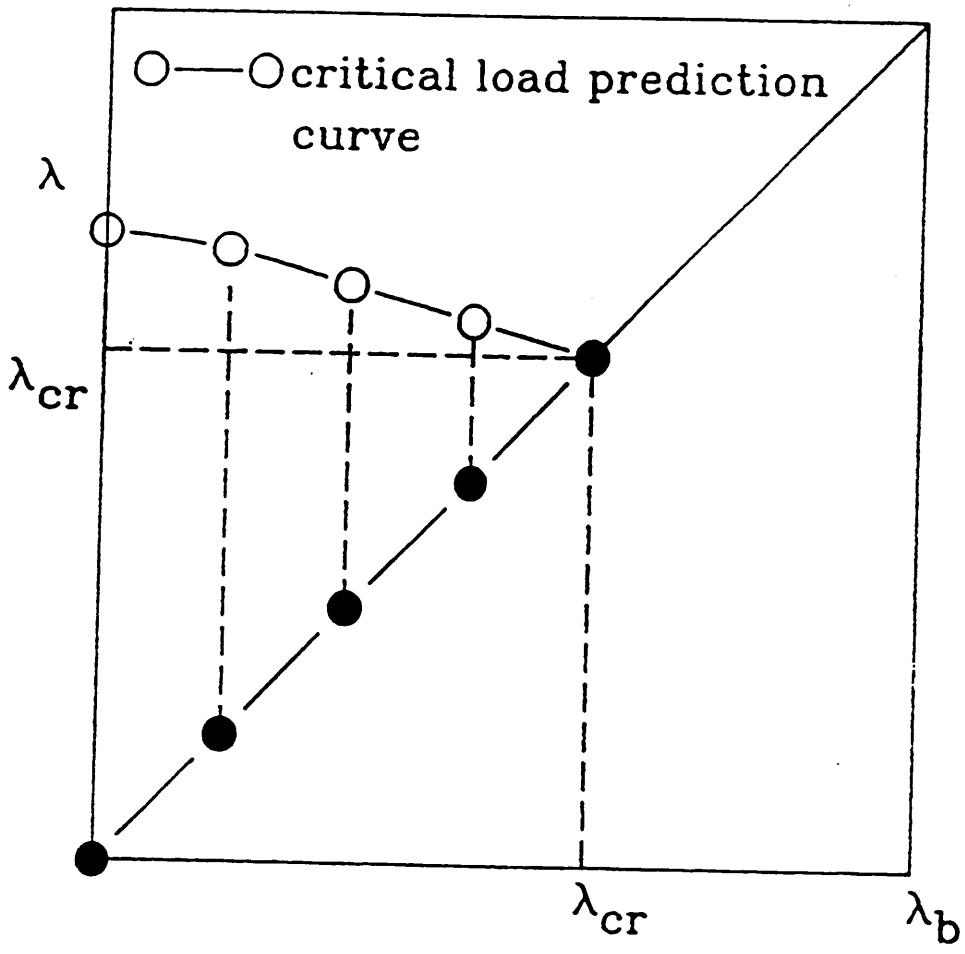

Figure 5.5.1 Buckling load prediction

An application of this method to an arch subject to single load distribution is presented in Fig. 5.5.2.

For a structure subject to multiple load distributions, the associated buckling load prediction is discussed in the following.

Assume the base load, ${}^{B}Q$, consists of contributions from both dead load, P_D, and live load, P_L. Then the base load is

$$ {}^{B}Q = P_D + \alpha P_L \tag{5.5.3} $$

where α is a scalar.

The load increment, ΔQ, is expressed as

$$ \Delta Q = \beta P_L \tag{5.5.4} $$

We notice from equation (5.5.4) that the load increment does not receive a contribution from the dead load because the dead load remains unchanged during the analysis.

The applied load, Q, is expressed as

$$ \begin{aligned} Q &= {}^{B}Q + \Delta Q \\ &= P_D + (\alpha + \beta) P_L \end{aligned} \tag{5.5.5} $$

If the corresponding eigenvalue is C_{cr}, then the corresponding predicted buckling load is

$$
\begin{aligned}
Q_{CR} &= {}^{B}Q + C_{cr}\,\Delta Q \\
&= (P_D + \alpha P_L) + C_{cr}\,(\beta P_L) \\
&= P_D + (\alpha + C_{cr}\beta)\,P_L
\end{aligned}
\tag{5.5.6}
$$

Let $\lambda_{CR} = \alpha + C_{cr}\beta$ and $\lambda_B = \alpha + \beta$. We rewrite equations (5.5.5) and (5.5.6) as follows :

$$Q_B = P_D + \lambda_B P_L \tag{5.5.7}$$

$$Q_{CR} = P_D + \lambda_{CR} P_L \tag{5.5.8}$$

When λ_B approaches the actual λ_{CR}, the predicted buckling load converges to the actual buckling load. Using the same extrapolation method we use for single load distribution, we find the predicted λ_{CR}.

An application of this method to an arch subject to multiple load distributions is illustrated in Fig. 5.5.3.

5.6 Nonlinear analysis with ABAQUS

Since the location of a critical point on the equilibrium path is not known *apriori*, very often nonlinear analyses are either terminated before the buckling load is reached or beyond the buckling load. Accordingly it is useful to obtain an estimate of the location of the critical point from initial buckling load predictions.

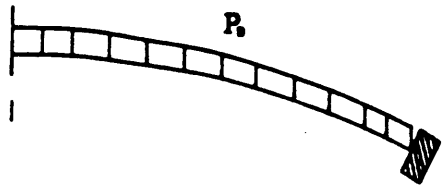

P_i	P_j	C_{cr}	P_{cr}
-500	-10	73.644	-1236.44
-600	-10	58.559	-1185.59
-700	-10	43.399	-1133.99
-800	-10	27.934	-1079.34
-900	-10	13.038	-1030.38

Note :

P_j, the load increment, is -100.

C_{cr} is the first eigenvalue obtained from ABAQUS output

P_{cr} is found to be between -968 and -971 from a nonlinear analysis

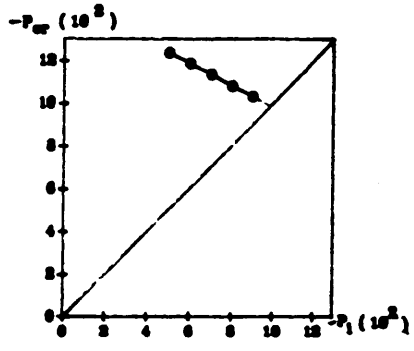

Figure 5.5.2 Buckling prediction for single load distributions (Arch)

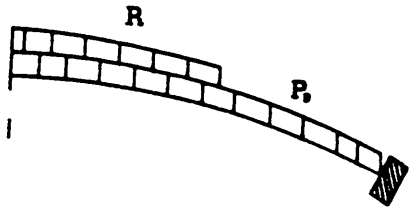

α	β	P_1	C_{Cr}^*	λ_B $= \alpha + \beta$	λ_{Cr} $= \alpha + C_{Cr}\beta$	P_{Cr}
0	0.1	-500	80.192	0.1	8.0192	-1301.92
1	0.1	-600	66.037	1.1	7.6037	-1260.37
2	0.1	-700	51.788	2.1	7.1788	-1217.88
3	0.1	-800	37.28	3.1	6.728	-1172.8
4	0.1	-900	23.214	4.1	6.3214	-1132.14

Note :

$P_1 = P_0 + \alpha P_L$

$P_1 = \beta P_L$

$P_0 = -500$

$P_L = -100$

$P_{Cr} = P_0 + \lambda_{Cr} P_L$

C_{Cr} is the first eigenvalue obtained from ABAQUS output

P_{Cr} is found to be -1055 from a nonlinear analysis

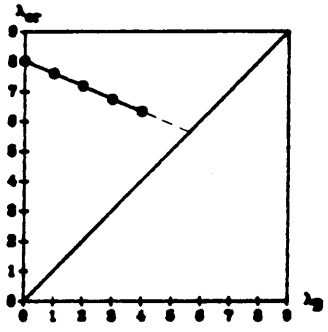

Figure 5.5.3 Buckling prediction for multiple load distributions (Arch)

Usually the undeformed mesh can provide a quick check of the geometry of the model. Applying a set of simplified loads, and comparing the results of analysis with the anticipated responses of the structure can often help in detecting the flaws in the geometry, material properties, and boundary conditions. In addition, the deformed mesh can help in localizing the modelling errors.

Once the model passes all tests mentioned above, we conduct a linear analysis, and study the result to verify the applied load vector. Moreover we check the element stresses against the design code at this stage.

Having performed the linear analysis, we conduct the buckling load prediction. We apply the base load, Q_B , first, then add the load increment ΔQ , and obtain the corresponding eigenvalue as described in the section 5.5.

Once we have a prediction for λ_{CR} , we select the parameters that are used in the nonlinear analysis, specifically, the maximum load proportionality factor and the maximum number of increments. The analysis will stop when either the maximum load proportionality factor or the maximum number of increments is reached provided there is no system error such as insufficient disk space for output, insufficient CPU time, etc.. In addition, the analysis can be stopped once a limiting displacement of a certain node at a certain degree of freedom is reached.

Generally the fewer increments are allowed, the larger the load increment, ΔQ , in the Newton-Raphson method becomes. A large ΔQ often requires more iterations for the unbalanced force to meet the error tolerance specified. The force error tolerance is suggested to be 1 % of the maximum value of the applied load; the moment error tolerance is suggested to be the force error tolerance multiplied by the length

of the beam elements (ABAQUS, 1989). Furthermore, to control the accuracy of the load proportionality factor, λ, we specify the maximum increment in the load proportionality factor.

The buckling load prediction procedure discussed in the section 5.5 can provide the load parameters to perform a nonlinear analysis with reasonable cost. Figure 5.6 illustrates the steps one should take in a nonlinear analysis.

Because nonlinear analysis for a large model is very expensive, it is an economical necessity to use a simplified model which contains all the characteristics of the actual model to detect the flaws in the modelling as well as the options used in the analysis.

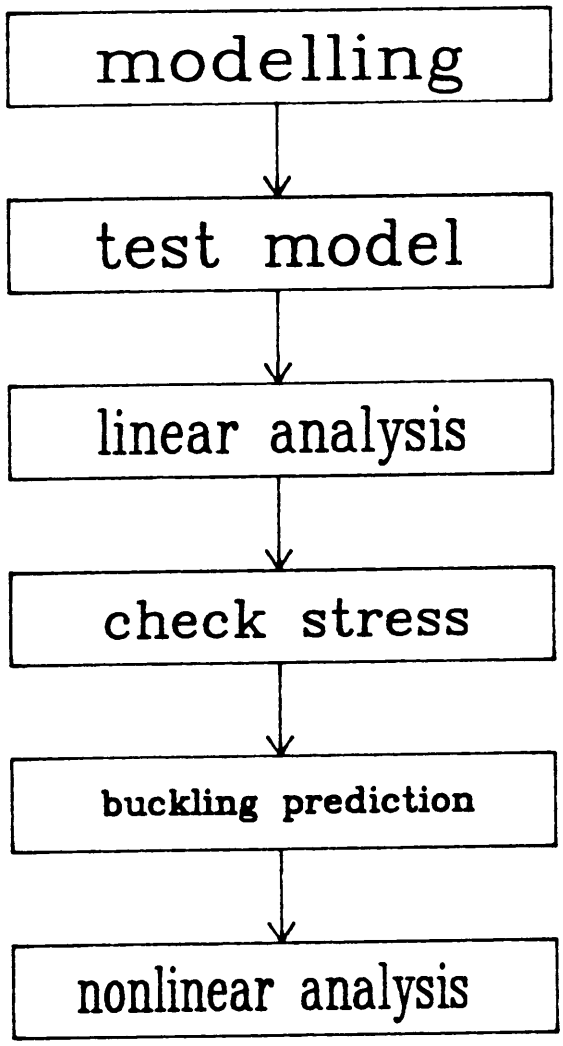

Figure 5.6 Nonlinear analysis with ABAQUS

CHAPTER 6 Stress Checking

6.1 Introduction

To check if the induced element stresses exceed the criteria defined in the National Design Specification, NDS, the stresses obtained from the ABAQUS analyses have to be separated into the axial and bending components first. For bending and axial tension, the formulas in Section 3.10.1 are applied. For bending and axial compression, the formulas in Section 3.10.2 are applied. A Fortran program for checking the element stresses obtained from ABAQUS output against NDS code is included in appendix C.

6.2 Separation of stresses

Consider a cross section of an element subject to an axial load and biaxial bending moments as shown in Fig. 6.2.1. Also let points 1, 2, 3, and 4 be the four corners of the cross section.

The axial stresses with a value A are developed at points 1, 2, 3, and 4 if an axial load is applied to this element. The bending stresses with a value B_1 at points 3 and 4 and with a value $-B_1$ at points 1 and 2 are developed if a bending moment is applied about the 1 axis of the cross section. The bending stresses with a value B_2 at points 1 and 3 and with a value $-B_2$ at points 2 and 4 are developed if a bending moment is applied about the 2 axis of the cross section.

The resultant stresses at the four corners, shown in Fig. 6.2.1, also can be expressed as

$$S_1 = A - B_1 + B_2 \tag{6.2.1}$$

$$S_2 = A - B_1 - B_2 \tag{6.2.2}$$

$$S_3 = A + B_1 + B_2 \tag{6.2.3}$$

$$S_4 = A + B_1 - B_2 \tag{6.2.4}$$

Equations 6.2.1-4 yield the relations for the stress components

$$A = \frac{1}{4}(S_1 + S_2 + S_3 + S_4) \tag{6.2.5}$$

$$B_1 = \frac{1}{4}(-S_1 - S_2 + S_3 + S_4) \tag{6.2.6}$$

$$B_2 = \frac{1}{4}(S_1 - S_2 + S_3 - S_4) \tag{6.2.7}$$

which follow from the conditions

$$\sum_{i=1}^{4} S_i = 4A \tag{6.2.8}$$

or

$$S_1 + S_2 = 2A - 2B_1 \tag{6.2.9}$$

$$S_3 + S_4 = 2A + 2B_1 \tag{6.2.10}$$

and

$$S_1 + S_3 = 2A + 2B_2 \tag{6.2.11}$$

$$S_2 + S_4 = 2A - 2B_2 \tag{6.2.12}$$

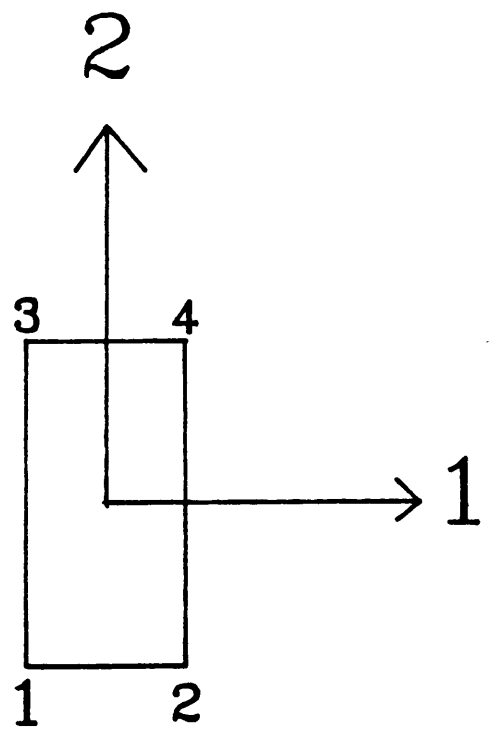

Figure 1. Fig. 6.2.1 Stress Separation

6.3 Checking the combined tensile and bending stresses

The design criteria for members subject to both bending and axial tension are (NDS, 1986)

$$\frac{f_t}{F_t} + \frac{f_b}{F_b} \leq 1 \qquad (6.3.1)$$

and

$$\frac{f_b - f_t}{F_b'} \leq 1 \qquad (6.3.2)$$

where

f_b = the actual stress at the extreme fiber in bending

f_t = the actual stress in tension parallel to grain

F_t = the design value in tension parallel to grain

F_b = the design value for extreme fiber in bending

F_b' = the design value for extreme fiber in bending adjusted by slenderness factor

In addition, NDS Section 5.3.4 requires F_b to be modified by a size factor if the glulam member is deeper than 11 inches. However, there is no member in this study deeper than 11 inches; therefore, Section 5.3.4 does not apply. The slenderness factor is discussed in NDS Section 3.3.3..

6.3.1 Adjusted design value for extreme fiber in bending

Based on the value of the slenderness factor, C_c, the adjusted design value for extreme fiber in bending, F_b', is derived from F_b.

NDS Section 3.3.3 states that the slenderness factor is computed as

$$C_c = \sqrt{\frac{l_e\, d}{b^2}} \qquad (6.3.3)$$

and C_c shall not exceed 50, where

b = the width of the beam

d = the depth of the beam

l_e = the effective length of the beam

According to NDS 3.3.3, the effective length is computed as

$$l_e = 1.84\, l_u \quad \text{if} \quad l_u/d \geq 14.3 \qquad (6.3.4)$$

and

$$l_e = 1.63l_u + 3d \quad if \quad l_u/d < 14.3 \tag{6.3.5}$$

where l_u is the laterally unsupported span of a bending member

Once the value of the slenderness ratio of a member is known, F_b' of the member is computed as follows

$$F_b' = F_b \quad if \quad C_c \leq 10 \tag{6.3.6}$$

$$F_b' = F_b \left[1 - \frac{1}{3} \left(\frac{C_c}{C_k} \right)^4 \right] \quad if \quad 10 < C_c \leq C_k \tag{6.3.7}$$

or

$$F_b' = 0.438 \frac{E}{C_c^2} \quad if \quad C_k < C_c \leq 50 \tag{6.3.8}$$

and

$$C_k = 0.811 \sqrt{\frac{E}{F_b}} \tag{6.3.9}$$

were E is Young's modulus, which is 1,800,000 for E-rated 56 southern pines.

NDS also requires that in no case can F_b' be greater than F_b.

6.4 Checking the combined compressive and bending stresses

Stated in NDS3.10.2, the design criterion for a member subject to both bending and compression is

$$\frac{f_c}{F_c'} + \frac{f_b}{F_b' - J f_c} \leq 1 \qquad (6.4.1)$$

where

f_c = the actual stress in compression parallel to grain

F_c' = the design value in compression parallel to grain adjusted by slenderness ratio

f_b = actual stress at extreme fiber in bending

F_b' = the design value for extreme fiber in bending adjusted by slenderness factor

J = a unitless convenience factor

and

$$J = \frac{(l_e/d) - 11}{K - 11} \qquad (6.4.2)$$

$$K = 0.671\sqrt{\frac{E}{F_c}} \qquad (6.4.3)$$

and $0 \leq J \leq 1$

The values of both K and F_c' of a member are dependent on the value of its slenderness ratio, l_e/d , as defined in NDS Section 3.7. The value of F_b' of the member was previously discussed.

6.4.1 Slenderness ratio in compression and adjusted design compressive strength

The value of the slenderness ratio of a member, l_e / d , determines the adjusted design value in compression parallel to grain, F_c'. The slenderness ratio is obtained by dividing the effective length, l_e , of the member by its depth. The effective length is obtained by multiplying the actual length of a member by its effective buckling length factor, k . The effective buckling length factor is dependent upon the end constraints of the member under consideration as described in NDS Appendix N. In this study, k is chosen to be 0.8.

The adjusted design value in compression parallel to grain is computed as follows :

$$F_c' = F_c \quad if \quad l_e/d \leq 11 \qquad (6.4.4)$$

$$F_c' = F_c \left[1 - \frac{1}{3} \left(\frac{l_e/d}{K} \right)^4 \right] \quad \text{if} \quad 11 < l_e/d < K \qquad (6.4.5)$$

$$F_c' = \frac{0.30\,E}{(l_e/d)^2} \quad \text{otherwise} \qquad (6.4.6)$$

CHAPTER 7 Results of analyses

7.1 Overview and load conditions analyzed

Three load combinations are analyzed, dead load and snow load (Fig. 3.3.1), dead load and inner snow load (Fig. 3.3.4), and dead load and outer snow load (Fig. 3.3.5). The dead load pressure is 16 psf and the snow load pressure is 20 psf. Linear analyses are performed for both the complete dome and the symmetrical substructure, a sector. B32 beam elements and C1D2 truss elements of ABAQUS are used to model the wood members and the steel tension ring. The boundary conditions are defined in section 4.5 for the complete dome, and in section 2.7 for the sector. The material properties are :

Young's modulus is 1,800,000 psi for glulam member

shear modulus is 160,000 psi for glulam member

Young's modulus is 29,000,000 psi for steel tension ring

7.2 Results of linear analyses

For all the three load conditions analyzed, the nodal displacements and element stresses of the complete dome and its substructure, a sector, are virtually identical.

For the combination of dead load and snow load (Fig. 3.3.1), the maximum vertical displacement is 1.8 in at the apex (node 1) of the dome, the maximum compressive stress observed is 1240 psi (allowable compressive stress is 2400 psi for this member) at the extreme fiber of the element 189, and the maximum tensile stress is 815 psi (allowable tensile stress is 1550 psi for this member) at the extreme fiber of the element 299. The nodes and members mentioned above are shown in Fig 7.2.4. No member fails to meet the combined stress requirements of the NDS code. The top and side views of the deformed mesh are shown in Fig. 7.2.1.

For the combination of dead load and inner snow load (Fig. 3.3.4), the maximum vertical displacement is 1.78 in at the apex (node 1) of the dome, the maximum compressive stress observed is 902.7 psi (allowable compressive stress is 2400 psi for this member) at the extreme fiber of the element 178, and the maximum tensile stress is 592.45 psi (allowable tensile stress is 1550 psi for this member) at the extreme fiber of the element 299. The nodes and members mentioned above are shown in Fig 7.2.4. No member fails to meet the combined stress requirements of the NDS code. The top and side views of the deformed mesh are shown in Fig. 7.2.2.

For the combination of dead load and outer snow load (Fig. 3.3.5), the maximum vertical displacement is 1.15 in at the apex (node 1) of the dome, the maximum compressive stress observed is 953.60 psi (allowable compressive stress is 2400 psi for this member) at the extreme fiber of the element 189, and the maximum tensile stress is 596.85 psi (allowable tensile stress is 1550 psi for this member) at the extreme fiber of the element 300. The nodes and members mentioned above are shown in Fig 7.2.4. No member fails to meet the combined stress the requirements of NDS code. The top and side views of the deformed mesh are shown in Fig. 7.2.3.

It is interesting that the critical load condition for the buckling is the outer snow load, while the critical load condition in the linear range (based on stress) is unform snow load over the entire dome.

7.3 Results of nonlinear analyses

For each load combination, we perform the eigenvalue prediction (section 5.8) and nonlinear analysis. The force error tolerance is 1 % of the maximum value of the discretized loads, the moment error tolerance is the force error tolerance multiplied by the element length, and the maximum load proportionality factor increment is 0.2.

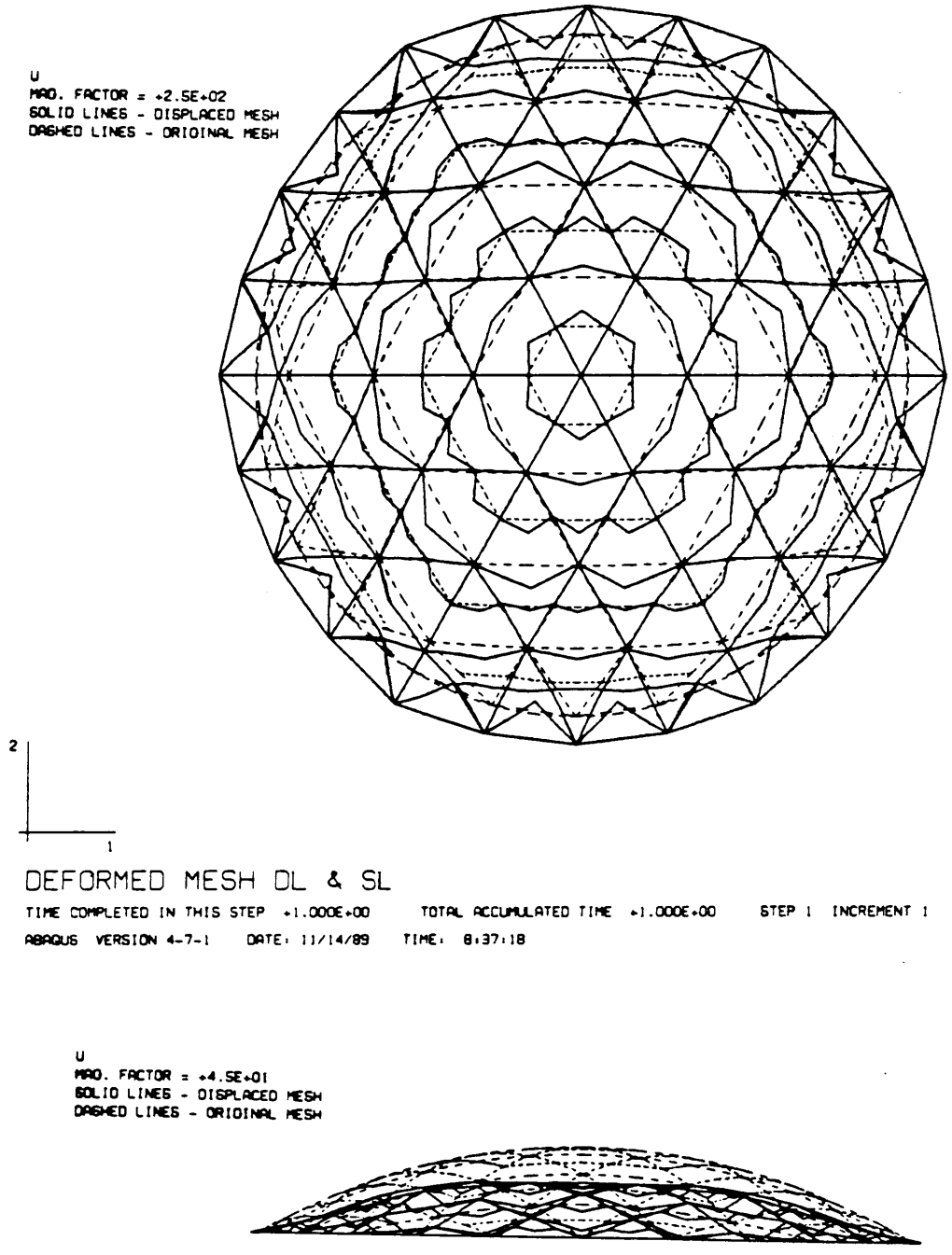

Figure 7.2.1 Deformed mesh of the dome under dead load and snow load

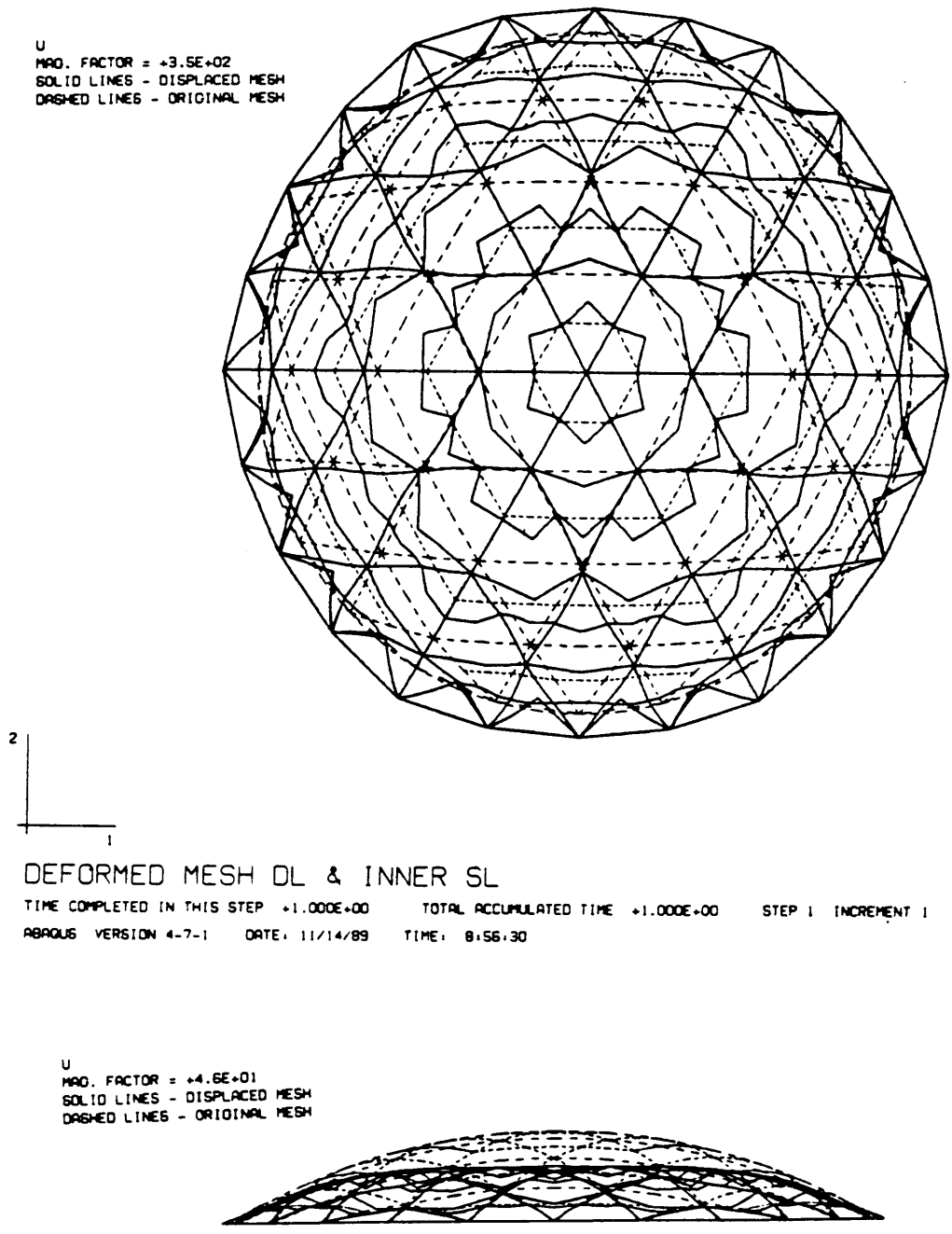

Figure 7.2.2 Deformed mesh of the dome under dead load and inner snow load

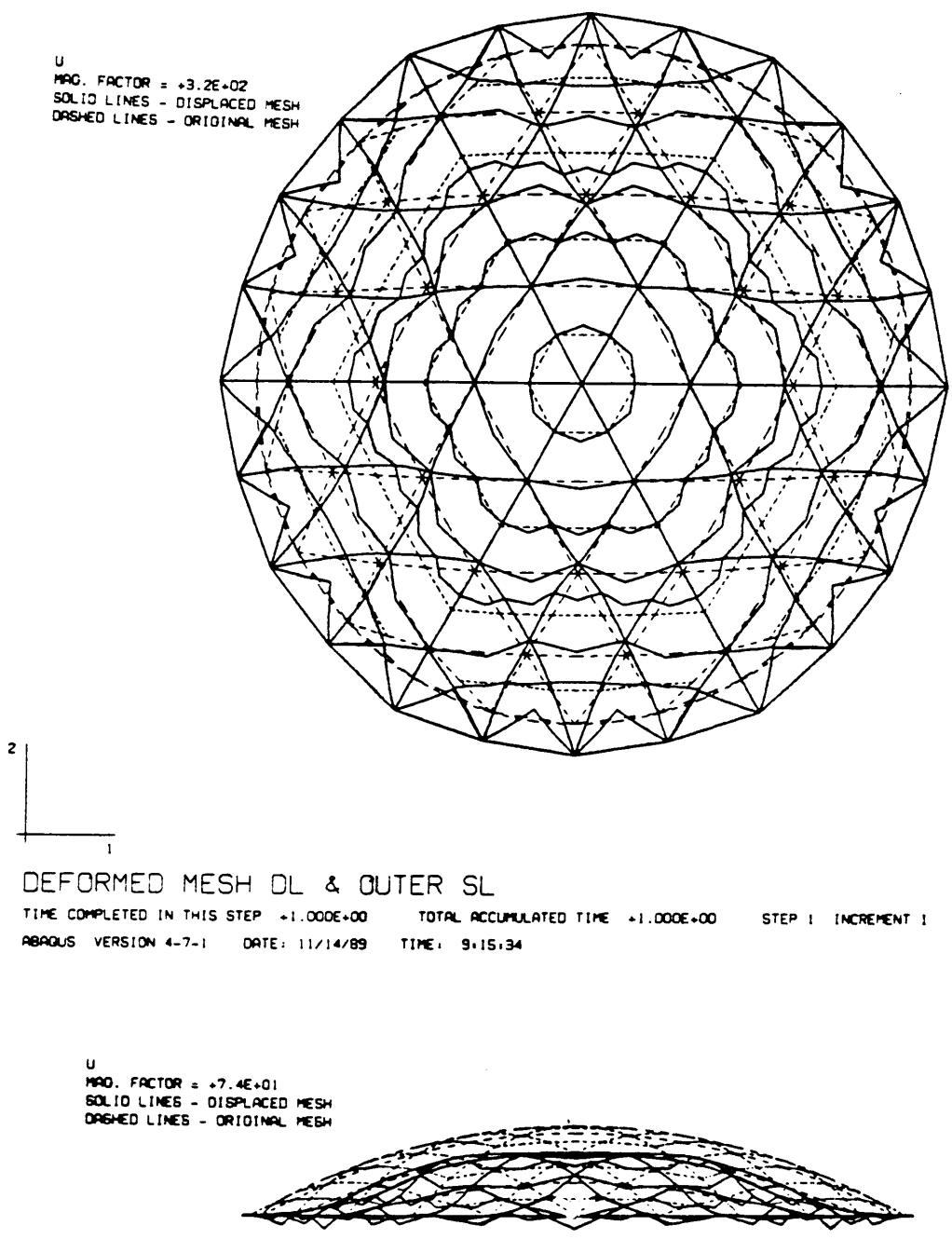

Figure 7.2.3 Deformed mesh of the dome under dead load and outer snow load

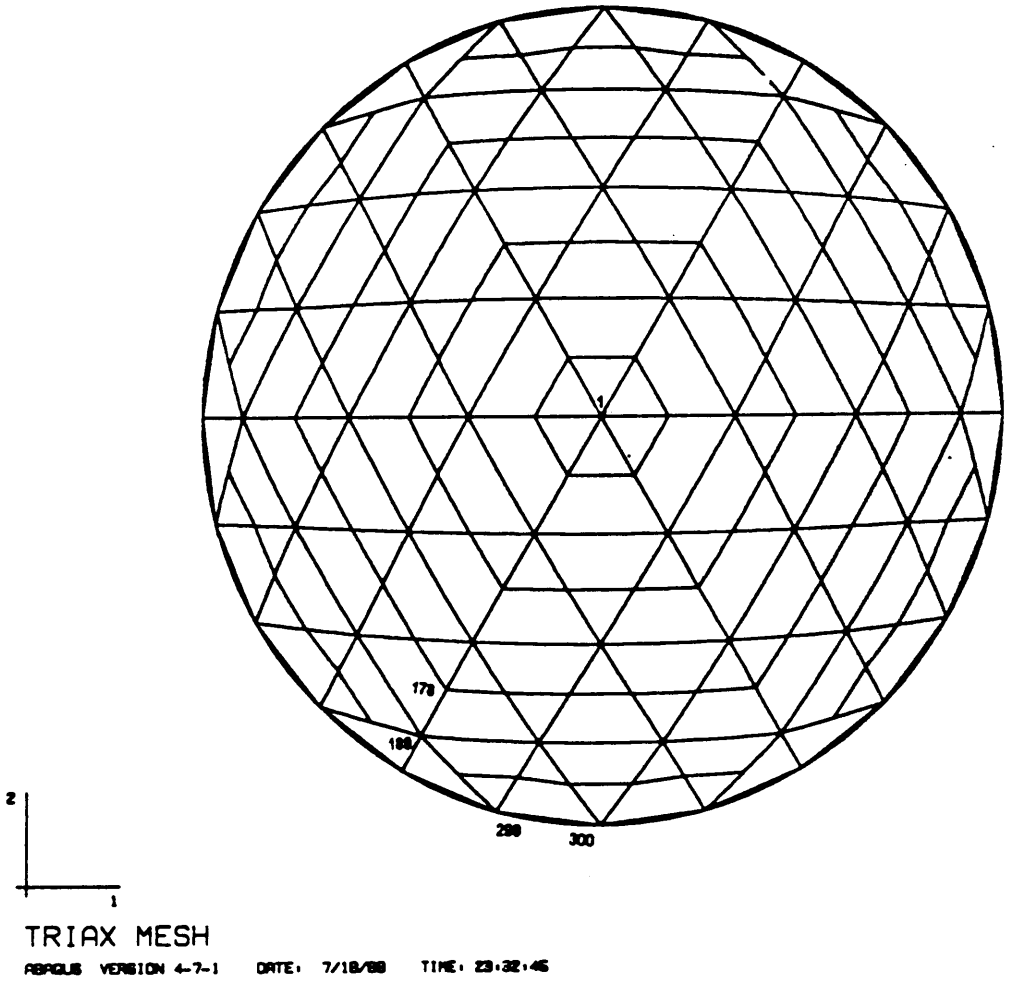

Figure 7.2.4 Critical nodes and elements

The results of the computation of buckling load predictions is shown in Table 7.3.1, Table 7.3.2 and Table 7.3.3 for the combination of dead load and snow load, the combination of dead load and inner snow load, and the combination of dead load and outer snow load.

The predicted buckling loads are shown in Fig. 7.3.1, Fig. 7.3.2, and Fig. 7.3.3 for the combination of dead load and snow load, the combination of dead load and inner snow load, and the combination of dead load and outer snow load.

Table 7.3.1

Buckling load prediction for the combination of dead load and snow load

α	β	P_l	$C_{cr}^{\cdot}$	λ_s $= \alpha + \beta$	λ_{cr} $= \alpha + C_{cr}\beta$	P_{cr}
1	0.05	0.2500	69.09	1.05	4.45	0.73
2	0.05	0.3889	52.93	2.05	4.65	0.76
3	0.05	0.5278	37.18	3.05	4.86	0.79
4	0.05	0.6667	19.79	4.05	4.99	0.80

Note :

$P_l = P_D + \alpha P_L$

$P_l = \beta P_L$

P_D = 0.1111 lb / in^2 or 16 psf

P_L = 0.1389 lb / in^2 or 20 psf

C_{cr} is the first eigenvalue available from ABAQUS output

$P_{cr} = P_D + \lambda_{cr} P_L$

C_{cr} is found to be between 4.95 and 5.11 from the nonlinear analysis

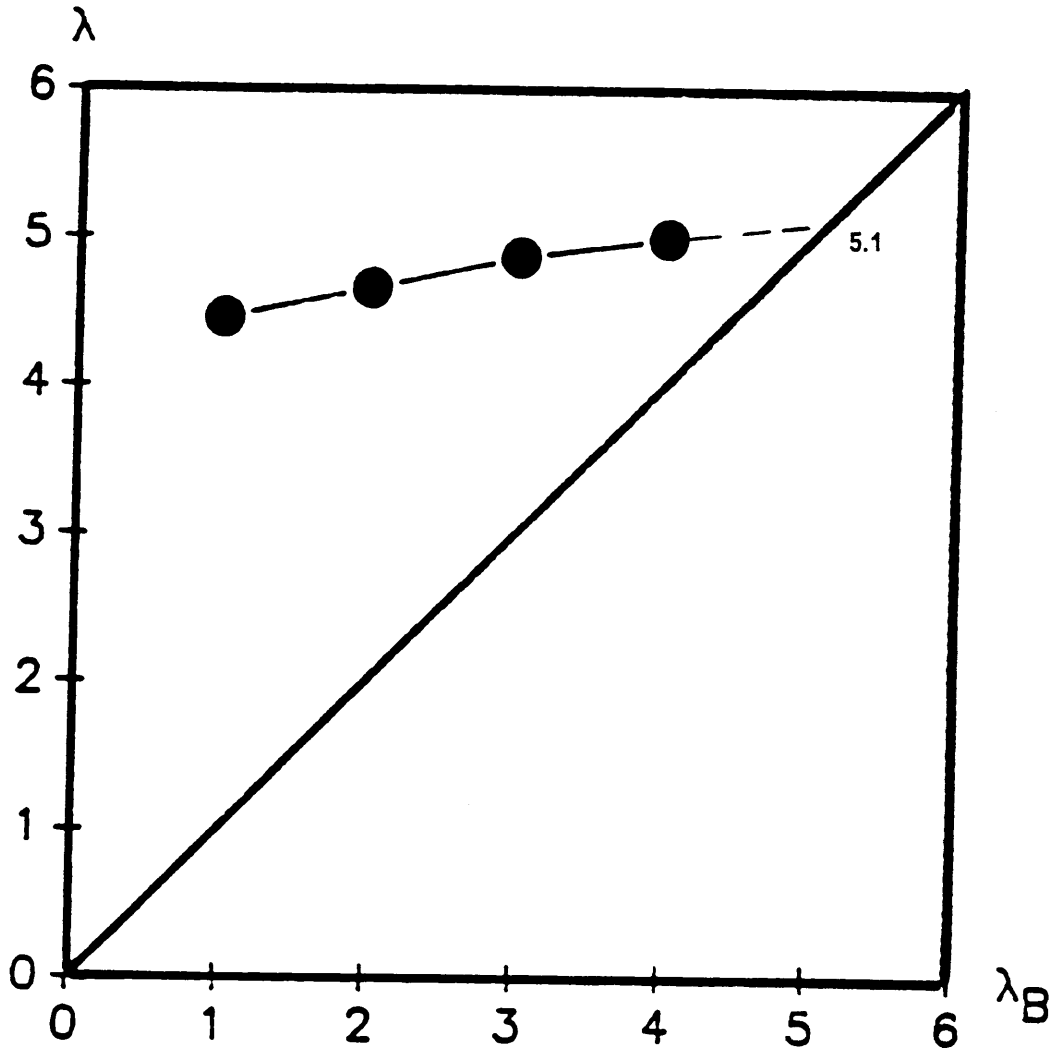

Figure 7.3.1 Buckling load prediction for dead load and snow load

Table 7.3.2

Buckling load prediction:the combination of dead load and inner snow load

α	β	P_I	C_{cr}	$\lambda_s = \alpha + \beta$	$\lambda_{cr} = \alpha + C_{cr}\beta$	P_{cr}
1	0.05	0.2500	77.16	1.05	4.86	0.79
2	0.05	0.3889	59.69	2.05	4.98	0.80
3	0.05	0.5278	42.92	3.05	5.15	0.83
4	0.05	0.6667	24.84	4.05	5.24	0.84

Note :

$P_I = P_D + \alpha P_L$

$P_I = \beta P_L$

P_D = 0.1111 lb / in^2 or 16 psf

P_L = 0.1389 lb / in^2 or 20 psf

C_{cr} is the first eigenvalue available from ABAQUS output

$P_{cr} = P_D + \lambda_{cr} P_L$

C_{cr} is found to be between 5.28 and 5.29 from the nonlinear analysis

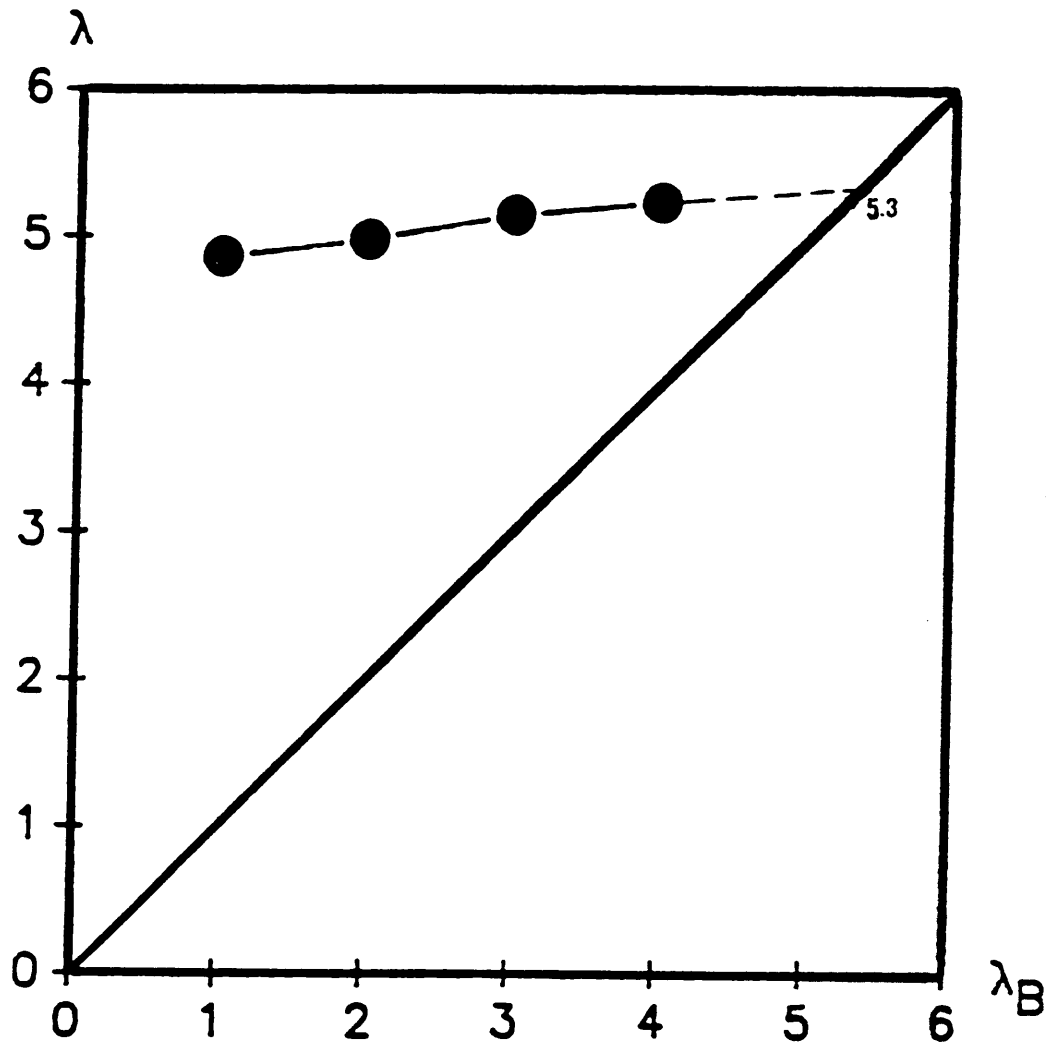

Figure 7.3.2 Buckling load prediction for dead load and inner snow load

Table 7.3.3

Buckling load prediction:the combination of dead load and outer snow load

α	β	P_l	C_{cr}	$\lambda_s = \alpha + \beta$	$\lambda_{cr} = \alpha + \beta C_{cr}$	P_{cr}
1	0.05	0.2500	78.31	1.05	4.97	0.80
2	0.05	0.3889	55.93	2.05	4.80	0.78
3	0.05	0.5278	34.23	3.05	4.71	0.77
4	0.05	0.6667	12.08	4.05	4.60	0.75

Note :

$P_l = P_D + \alpha P_L$

$P_l = \beta P_L$

P_D = 0.1111 lb / in^2 or 16 psf

P_L = 0.1389 lb / in^2 or 20 psf

C_{cr} is the first eigenvalue available from ABAQUS output

$P_{cr} = P_D + \lambda_{cr} P_L$

C_{cr} is found to be between 4.60 and 4.61 from the nonlinear analysis

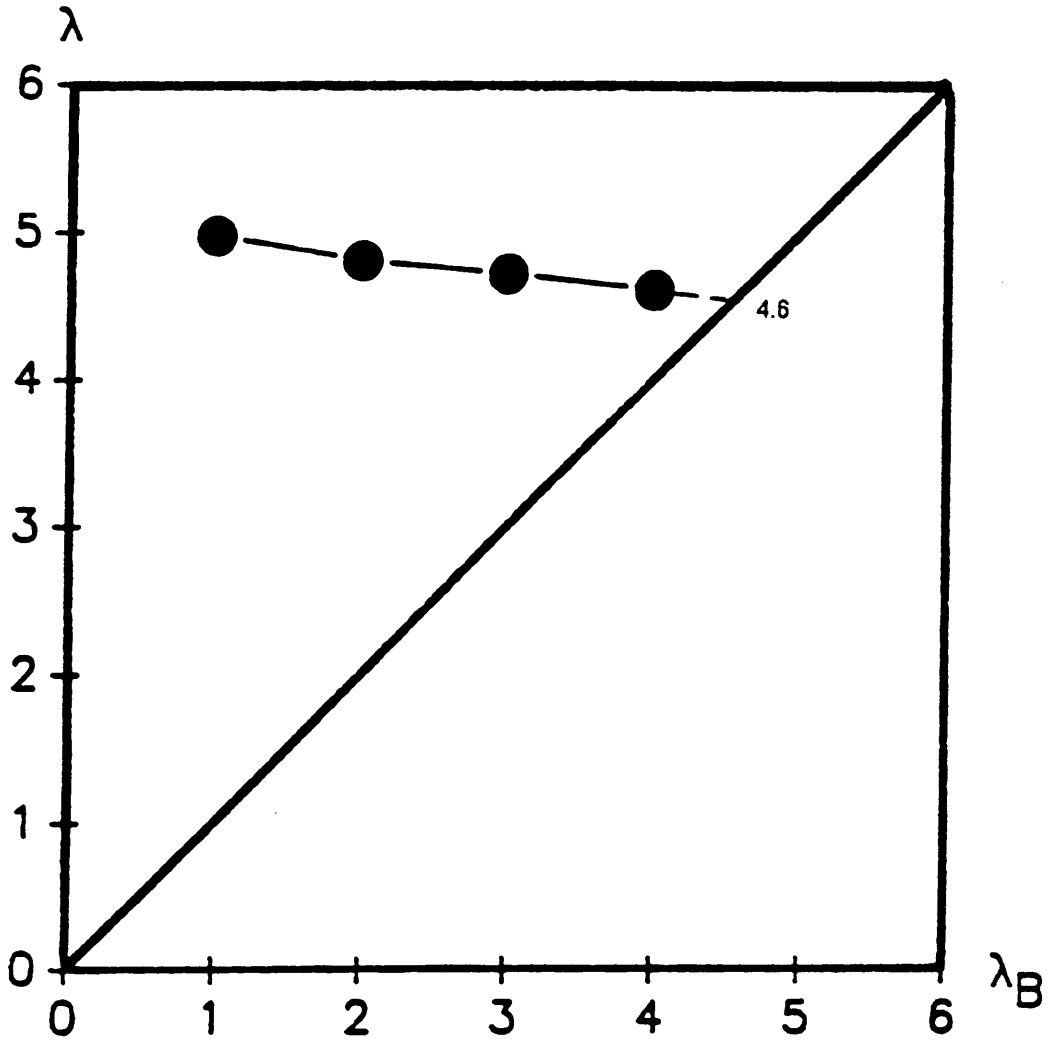

Figure 7.3.3 Buckling load prediction for dead load and outer snow load

CHAPTER 8 Conclusion and recommendation

8.1 Conclusion

The application of symmetry principle is proven to be effective in linear analysis; however, its application in nonlinear analysis is not satisfactory. The discrepancy in buckling predictions of the complete structure and the symmetrical sub-structure is caused by the suppression of the buckling modes (bifurcation modes) in the sub-structure (Davalos, 1989).

The buckling load prediction procedure is proven to be effective in the study; its application in multiple load conditions is especially interesting because of the relative low cost and reasonable accuracy. Furthermore it can provide the values of parameters used in the nonlinear analysis.

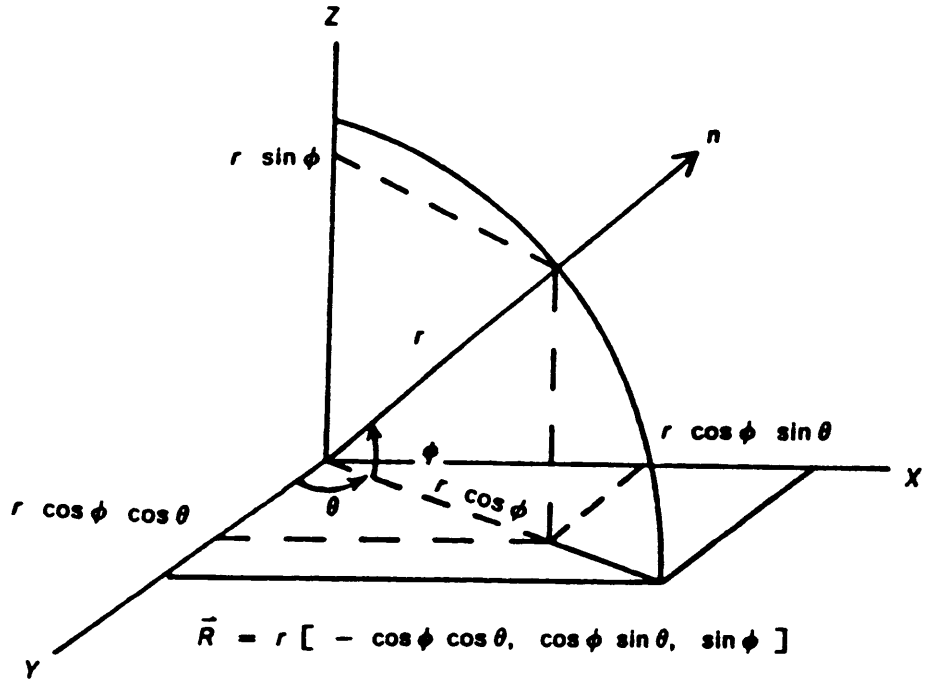

$$\vec{R} = r\,[\, -\cos\phi\cos\theta,\ \cos\phi\sin\theta,\ \sin\phi\,]$$

$$\vec{1} = \frac{1}{r}\frac{d\vec{R}}{d\phi}$$

$$= [\, -\sin\phi\cos\theta,\ -\sin\phi\sin\theta,\ \cos\phi\,]$$

or

$$\vec{1} = \frac{1}{r}\frac{d\vec{R}}{d\theta}$$

$$= [\, -\cos\phi\sin\theta,\ \cos\phi\cos\theta,\ 0\,]$$

Figure 8.1 Element local $\vec{1}$ in the polar coordinate system

8.2 Recommendation

Future research may be considered in the areas of experimental verification of mathematical modelling, computational accuracy, computational efficiency, and the development of time-saving preprocessors and postprocessors.

To improve the mathematical model, rigid joints can be replaced by flexible joints, and the decking can be modelled with shell elements. The variation in the strength of glulam members is expected to lower the buckling load of the dome because of the loss in the symmetry. Therefore, the effects of the variation in material properties are recommended for future research.

To improve the computational accuracy, a polar coordinate system is recommended to define the geometry of the dome. The mathematical expression of the local 1 axis of an element is included in Fig. 8.2.

Methods of improving the computational efficiency includes the study of the *substructures*, in which the critical elements are modelled nonlinearly; other elements are modelled linearly to save computational time.

A preprocessor capable of generating and refining the mesh, and performing load discretization is urgently needed. Several commercial codes including Ideas and Patran are preprocessors for the dome.

The interface between ABAQUS and user defined Fortran programs should be studied and employed in order to examine the dome against design codes at the user's specified load levels.

REFERENCES

ABAQUS, Hibbitt, Karlsson & Sorensen, Inc., 100 Medway Street, Providence, RI.

American Institute of Timber Construction, *Timber Construction Manual*, 3rd ed., John Wiley & Sons, Inc., New York, 1985.

Bathe, K. J., *Finite Element Procedures in Engineering Analysis*, Prentice-Hall, Englewood Cliffs, NJ, 1982.

Chang, S. C., and Chen, J., J., " Effectiveness of Linear Bifurcation Analysis for Predicting the Nonlinear Stability Limits of Structures, " International Journal for Numerical Methods in Engineering, Vol. 23, 1980, pp. 831-846

Davalos, J. F., "Background for Finite Element Analysis and Experimental Testing of Glued-Laminated Space Beams," M.S. Thesis, Virginia Polytechnic Institute and State University, July 1987.

Davalos, J. F., "Geometrically Nonlinear Finite Element Analysis of a Glulam Timber Dome" Ph. D. Dissertation, Virginia Polytechnic Institute and State University, July 1989.

Holzer, S. M. and Loferski, J. R., "Background for Research on Glulam Lattice Domes," *Proceedings of the Sixth Annual Structures Congress*, ASCE Structural Division, Orlando, FL, August 1987, pp. 305-318.

Holzer, S. M., *Computer Analysis of Structures*, Elsevier, New York, NY, 1985

Holzer, S. M., Watson, L. T., and Vu, P., "Stability Analysis of Lamella Domes," *Proceedings of the ASCE Symposium on Long Span Roof Structures*, St. Louis, MO, October 1981, pp. 179-209.

Neal, D. W., *The Triax Dome*, Culbertson, Noren, and Neal, Consulting Engineers, 1410 S. W. Morrison St., Portland, OR 97205, March 1973.

Varex Domes, Western Wood Structures Inc., Tualatin, Oregon.

Appendix A

```
C     THE PROGRAM COMPUTES NODAL FORCES AT EACH NODE OF EVERY PANEL
C     OF THE TRIAX DOME
C     FROM ALL THE ADJACENT PANELS ( NOT INCLUDED IN THIS PROGRAM)

C     EACH PANEL IS DIVIDED INTO TWO PARTS, THE CORRESPONDING
C     PRESSURES OVER EACH PART ARE PRESENTED BY COEFFICIENTS P(1,NOPL)
C     AND P(2,NOPL).

C     15 NODES/ PANEL.

C     THE NODAL FORCE INDUCED BY P(1,NOPL) AT NODE J IS REPRESENTED AS
C     A(J,NOPL) AND B(J,NOPL) IS THE NODAL FORCE INDUCED BY P(2,NOPL)
C     WHERE J IS LOCAL NODE NUMBER AND NOPL IS THE PANEL NUMBER

      REAL A(15,96), B(15,96), P(2,96), FZ(15,96)

      DO 10 I = 1,96
        READ (2,*) NOPL, (A(J,NOPL), J = 1,15)
        READ (3,*) NOPL, (B(K,NOPL), K = 1,15)
        READ (4,*) NOPL, (P(L,NOPL), L = 1,2)
10    CONTINUE

      DO 20 J = 1,96
        DO 30 K = 1,15
```

```
            FZ(K,J) = P(1,J)*A(K,J) + P(2,J)*B(K,J)
30        CONTINUE
          WRITE(5,5) J, (FZ(L,J), L = 1,15)
5         FORMAT (I2,15(1X,F7.1))
20      CONTINUE

        END
```

Appendix B

```
      PARAMETER (NOTRL = 100, NDINTRL = 15, NDNO = 1000)

      INTEGER M(NDINTRL,NOTRL)
      REAL PX(NDNO), PY(NDNO), PZ(NDNO)
      REAL XFCTRL(NDINTRL,NOTRL),YFCTRL(NDINTRL,NOTRL),
     &     ZFCTRL(NDINTRL,NOTRL)
C*****************************************************************
C     PREPROCESSOR: READ MEMBER INCIDENCE
C                   READ PANEL LOAD VECTOR
C*****************************************************************
        DO 2 J = 1,96
        READ (2,*) NTR,(M(I,NTR), I = 1,15)
2       CONTINUE

        NTRGL = 96
        NDDX = 15

        DO 6 I = 1, NTRGL
        READ (5,*) NTR,(ZFCTRL(J,NTR), J = 1,NDDX)
6       CONTINUE


      DO 20 I = 1,NTRGL
```

```
      DO 30 J = 1,NDDX
         NDGL = M(J,I)
         IF (NDGL.NE.0) THEN
            PZ(NDGL) = PZ(NDGL) + ZFCTRL(J,I)
         END IF
30     CONTINUE
20   CONTINUE


     DO 40 I = 1,781
       IF (PZ(I).NE.0) THEN
          WRITE(8,5) I,',3,',PZ(I)
5         FORMAT (I5,A,E10.4)
       ENDIF
40   CONTINUE
```

Appendix C

```
PARAMETER (NOPT = 781, NOEL = 480)
REAL FT(2,NOEL), FB(2,NOEL), FC(2,NOEL)
REAL T1(2,NOEL), T2(2,NOEL), C(2,NOEL)
REAL S1(2,NOEL), S5(2,NOEL), S21(2,NOEL)
REAL AXI(2,NOEL), BND1(2,NOEL), BND2(2,NOEL), XJ(NOEL)
INTEGER MCODE(3,NOEL)
REAL COORD(3,NOPT), P(3,NOEL)
REAL XP(NOEL)
REAL CLE(NOEL), XLE(NOEL), CSR(NOEL), SR(NOEL), CS(NOEL)
REAL DFCPI(NOEL), DFBPI(NOEL), D(NOEL), B(NOEL)
READ ( 5,* ) CAP
WRITE(6,*) 'FAILURE DUE TO COMBINED BENDING AND TENSILE STRESSES'
WRITE(6,*) 'FAILURE DUE TO COMBINED BENDING AND TENSILE STRESSES'
WRITE(6.*) 'ELEMENT NO   GAUSSIAN PT NO   CAPACITY'
WRITE(7,*) 'FAILURE DUE TO COMBINED BENDING AND COMPRESSIVE STRESS
&ES'
WRITE(7,*) 'ELEMENT NO   GAUSSIAN PT NO   CAPACITY'

WRITE(8,*) 'ELEMENT SUBJECT TO TENSION'
WRITE(8,*) 'ELEMENT NO   GAUSSIAN PT NO   TENSILE STRESS'
WRITE(10,*)'       NEL       NPT  BND1 =              AXI = '
WRITE(11,*) NEL,NPT,'BND1(NPT,NEL) + AXI(NPT,NEL) = '

CALL PRE(COORD, MCODE, B, D)

DFT = 1550.
```

```
      DFB = 2400.


      E = 1.8E + 06
      DFC = 1850.
      CK = 0.67*(E/DFC)**0.5


      DO 10 I = 1, 124


        READ (1,*) NEL,NPT,NDUMMY,S1(NPT,NEL),DUMMY
        READ (1,*) NEL,NPT,NDUMMY,S5(NPT,NEL),DUMMY
        READ (1,*) NEL,NPT,NDUMMY,S21(NPT,NEL),DUMMY
        READ (1,*) NEL,NPT,NDUMMY,DUMMY1,DUMMY2


        AXI(NPT,NEL) =  0.5*S5(NPT,NEL) + 0.5*S21(NPT,NEL)
        BND1(NPT,NEL) =  -0.5*S1(NPT,NEL) + 0.5*S21(NPT,NEL)
        BND2(NPT,NEL) =  -0.5*S1(NPT,NEL) + 0.5*S5(NPT,NEL)


        WRITE(10,*) NEL,NPT,BND1(NPT,NEL),AXI(NPT,NEL)
        WRITE(11,*) NEL,NPT,BND1(NPT,NEL) + AXI(NPT,NEL)


10    CONTINUE


      DO 20 NEL = 1,NOEL
      IF (MCODE(1,NEL).NE.0) THEN
        DO 30 NPT = 1,2
        IF (AXI(NPT,NEL).GT.0.) THEN
```

```
      WRITE(8,25) NEL, NPT, AXI(NPT,NEL)
      FT(NPT,NEL) = AXI(NPT,NEL)
      FB(NPT,NEL) = ABS(BND1(NPT,NEL))
      CALL TENSILE(MCODE,COORD,P,XP,CLE,XLE,SR,CS,DFCPI,DFBPI,D,B,
     &NEL)
      T1(NPT,NEL) = FT(NPT,NEL)/DFT + FB(NPT,NEL)/DFB
      T2(NPT,NEL) = (FB(NPT,NEL)-FT(NPT,NEL))/DFBPI(NEL)
      IF (T1(NPT,NEL).GT.CAP) THEN
        WRITE(6,25) NEL, NPT, T1(NPT,NEL)
      END IF
      IF (T2(NPT,NEL).GT.CAP) THEN
        WRITE(6,25) NEL, NPT, T2(NPT,NEL)
      END IF



    ELSE IF (AXI(NPT,NEL).LE.0.) THEN
      FC(NPT,NEL) = ABS(AXI(NPT,NEL))
      FB(NPT,NEL) = ABS(BND1(NPT,NEL))
      CALL COMPRESS(MCODE,COORD,P,XP,CLE,CSR,SR,DFCPI,DFBPI,D,XJ,
     &NEL)
      C(NPT,NEL) = FC(NPT,NEL)/DFC + FB(NPT,NEL)/(DFB-XJ(NEL)*
     &FC(NPT,NEL))
      IF (C(NPT,NEL).GT.CAP) THEN
         WRITE(7,25) NEL, NPT, C(NPT,NEL)
      END IF
```

```
25      FORMAT (6X,I5,3X,I14,3X,F12.4)

        END IF
30      CONTINUE
        END IF
20    CONTINUE



      END
C
      SUBROUTINE PRE(COORD, MCODE, B, D)

      REAL COORD(3,*),B(*),D(*)
      INTEGER MCODE(3,*)

      DO 10 I = 1,781
        READ (2,*) ND, COORD(1,ND), COORD(2,ND), COORD(3,ND)
10    CONTINUE

      DO 20 I = 1,480
        READ(3,*) NELM,MCODE(1,NELM),MCODE(2,NELM),MCODE(3,NELM)
20    CONTINUE

      DO 30 I = 1,480
```

```
      READ(4,*) D(I), B(I)
30    CONTINUE


      RETURN

      END

C
      SUBROUTINE TENSILE(MCODE,COORD,P,XP,CLE,XLE,SR,CS,DFCPI,DFBPI,D,B,
     &NEL)

      REAL COORD(3,*), P(3,*)
      INTEGER MCODE(3,*)
      REAL XP(*)
      REAL CLE(*), XLE(*), SR(*), CS(*)
      REAL DFCPI(*), DFBPI(*), D(*), B(*)

      E = 1.8E + 06
      DFT = 1550.
      DFB = 2400.

      NE1 = MCODE(1,NEL)
      NE2 = MCODE(3,NEL)

      CK = 0.811*(E/DFB)**0.5
```

```
      DO 10 I = 1,3
        P(I,NEL) = COORD(I,NE2)-COORD(I,NE1)
10    CONTINUE

      XP(NEL) = (P(1,NEL)**2 + P(2,NEL)**2 + P(3,NEL)**2)**0.5
C     XP(NEL) = 2*XP(NEL)

      SR(NEL) = XP(NEL)/D(NEL)

      IF (SR(NEL).GT.14.3) THEN
        XLE(NEL) = 1.84*XP(NEL)
      ELSE
        XLE(NEL) = 1.63*XP(NEL) + 3*D(NEL)
      ENDIF

      CS(NEL) = (XLE(NEL)*D(NEL)/B(NEL)**2)**0.5

      IF (CS(NEL).GE.50.) THEN
        CS(NEL) = 50.
      ENDIF

      IF (CS(NEL).LE.10.) THEN
        DFBPI(NEL) = DFB
      ELSE IF (CS(NEL).LT.CK) THEN
```

```
      DFBPI(NEL) = DFB*(1.-1./3.*(CS(NEL)/CK)**4)
    ELSE
      DFBPI(NEL) = 0.438*E/CS(NEL)**2
    ENDIF

    RETURN
    END
C
    SUBROUTINE COMPRESS(MCODE,COORD,P,XP,CLE,CSR,SR,DFCPI,DFBPI,D,XJ,
   &NEL)

    REAL COORD(3,*), P(3,*)
    INTEGER MCODE(3,*)
    REAL XP(*), XJ(*)
    REAL CLE(*), CSR(*)
    REAL DFCPI(*), D(*)

    E = 1.8E + 06
    DFC = 1850.
    CK = 0.67*(E/DFC)**0.5

    NE1 = MCODE(1,NEL)
    NE2 = MCODE(3,NEL)

    DO 10 I = 1,3
```

```
      P(I,NEL) = COORD(I,NE2)-COORD(I,NE1)
10    CONTINUE

      XP(NEL) = (P(1,NEL)**2 + P(2,NEL)**2 + P(3,NEL)**2)**0.5
C     XP(NEL) = 2*XP(NEL)

      XKL = 0.80
      CLE(NEL) = XKL*XP(NEL)
      CSR(NEL) = CLE(NEL)/D(NEL)
      IF(CSR(NEL).LE.11.) THEN
        DFCPI(NEL) = DFC
      ELSE IF (11..LT.CSR(NEL).AND.CSR(NEL).LT.CK) THEN
        DFCPI(NEL) = DFC*(1.-1./3.*(CSR(NEL)/D(NEL)/CK)**4)
      ELSE
        DFCPI(NEL) = 0.3*E/(CLE(NEL)/D(NEL))**2
      END IF

      XJ(NEL) = (CSR(NEL)-11.)/(CK-11.)

      RETURN

      END
```

The vita has been removed from the scanned document